

**APPLICATION OF MODIFIED MAGNETIC BIOCHAR FOR  
DEGRADATION OF ORGANIC DYES USING ADVANCED  
OXIDATION PROCESSES**

**CATHERINE CHIN JIA XIN**

**A project report submitted in partial fulfilment of the  
requirements for the award of Bachelor of Engineering  
(Honours) Chemical Engineering**

**Lee Kong Chian Faculty of Engineering and Science  
Universiti Tunku Abdul Rahman**

**May 2021**

**DECLARATION**

I hereby declare that this project report is based on my original work except for citations and quotations which have been duly acknowledged. I also declare that it has not been previously and concurrently submitted for any other degree or award at UTAR or other institutions.

Signature : *Catherine*  
\_\_\_\_\_

Name : Catherine Chin Jia Xin  
\_\_\_\_\_

ID No. : 16UEB03493  
\_\_\_\_\_

Date : 5 May 2021  
\_\_\_\_\_

**APPROVAL FOR SUBMISSION**

I certify that this project report entitled “**APPLICATION OF MODIFIED MAGNETIC BIOCHAR FOR DEGRADATION OF ORGANIC DYES USING ADVANCED OXIDATION PROCESSES**” was prepared by **CATHERINE CHIN JIA XIN** has met the required standard for submission in partial fulfilment of the requirements for the award of Bachelor of Engineering (Honours) Chemical Engineering at Universiti Tunku Abdul Rahman.

Approved by,

Signature :   
\_\_\_\_\_

Supervisor : Pang Yean Ling

Date : 5 May 2021

Signature :   
\_\_\_\_\_

Co-Supervisor : Chong Woon Chan

Date : 5 May 2021

The copyright of this report belongs to the author under the terms of the copyright Act 1987 as qualified by Intellectual Property Policy of Universiti Tunku Abdul Rahman. Due acknowledgement shall always be made of the use of any material contained in, or derived from, this report.

© 2021, Catherine Chin Jia Xin. All right reserved.

## **ACKNOWLEDGEMENTS**

I would like to thank everyone who had contributed to the successful completion of this research project. First and foremost, I would like to express my gratitude to my research supervisor and co-supervisor, Dr Pang Yean Ling and Ir. Dr Chong Woon Chan for their invaluable advice, guidance and enormous patience throughout the development of the research.

In addition, I would also like to express my gratitude to my loving parents and friends who had helped and given me encouragement throughout this research period. I would also like to extend special thanks to my coursemates who had gave me necessary information and support in completing this whole project.

## ABSTRACT

Untreated wastewater released into the environment has caused water pollution for decades. Recently, researchers found that magnetic biochar could play a big role in combating water pollution especially textile wastewater due to its magnetic separation characteristic. In this study, various types of synthesis methods were analysed from multiple journal papers in the preparation of modified magnetic biochar. This study also established an understanding for the characterisation testings such as Scanning Electron Microscopy with Energy Dispersive X-ray Spectroscopy (SEM-EDX), Brunauer-Emmett-Teller (BET) surface area analysis, Fourier Transform Infrared spectroscopy (FTIR) and X-ray Diffraction (XRD) analysis. Besides, the catalytic mechanism of magnetic biochar catalysts in the Fenton process, photo-Fenton process, and photocatalysis process were summarized. The kinetic models were studied and found the most of the processes were followed pseudo-first order reaction. The reusability and stability of magnetic biochar catalysts with their degradation efficiencies in different oxidation processes were also evaluated. The present study proved that various types of biomass can be used as feedstocks in the preparation of magnetic biochar catalyst for degradation efficiency in organic dyes and able to achieve as high as 99.9 %.

## TABLE OF CONTENTS

<b>DECLARATION</b>		<b>i</b>
<b>APPROVAL FOR SUBMISSION</b>		<b>ii</b>
<b>ACKNOWLEDGEMENTS</b>		<b>iv</b>
<b>ABSTRACT</b>		<b>v</b>
<b>TABLE OF CONTENTS</b>		<b>vi</b>
<b>LIST OF TABLES</b>		<b>viii</b>
<b>LIST OF FIGURES</b>		<b>x</b>
<b>LIST OF SYMBOLS / ABBREVIATIONS</b>		<b>xi</b>
<b>CHAPTER</b>		
<b>1</b>	<b>INTRODUCTION</b>	<b>1</b>
1.1	Water Pollution in Malaysia	1
1.2	Textile Industry and Environmental Impact	2
1.3	Production and Classifications of Dyes	4
1.4	Removal Techniques	7
1.5	Problem Statement	10
1.6	Aim and Objectives	11
<b>2</b>	<b>LITERATURE REVIEW</b>	<b>12</b>
2.1	Biochar	12
2.2	Feedstocks of Biochar	14
2.3	Production of Biochar	19
2.3.1	Pyrolysis	19
2.3.2	Gasification	20
2.3.3	Hydrothermal Carbonization	22
2.4	Modification of Biochar	23
2.4.1	Nano-zerovalent Iron Modified Biochar	24
2.4.2	Carbonaceous Materials	26
2.4.3	Metal Oxides	27
2.5	Advanced Oxidation Process	30

	2.5.1 Photocatalysis	31
	2.5.2 Fenton and Fenton-like Processes	33
2.6	Parameter Study	36
	2.6.1 Effect of H <sub>2</sub> O <sub>2</sub> concentration	36
	2.6.2 Effect of Catalyst Dosage	37
	2.6.3 Effect of pH solution	37
	2.6.4 Effect of Initial Dye Concentration	38
<b>3</b>	<b>METHODOLOGY AND WORK PLAN</b>	<b>40</b>
3.1	Research Methodology	40
	3.1.1 Planning	40
	3.1.2 Searching	41
	3.1.3 Screening and Reporting	42
3.2	Data Collection	42
3.3	Data Analysis	44
<b>4</b>	<b>RESULTS AND DISCUSSION</b>	<b>45</b>
4.1	Synthesis of Magnetic Biochar	45
4.2	Characterisation of Magnetic Biochar	53
	4.2.1 Scanning Electron Microscope with Energy Dispersive X-Ray (SEM-EDX)	53
	4.2.2 Brunauer-Emmett-Teller (BET) Surface Area Analysis	55
	4.2.3 X-Ray Diffraction (XRD) Analysis	56
	4.2.4 Fourier Transform Infrared Spectroscopy (FTIR)	58
4.3	Mechanism for Dye Removal	59
4.4	Kinetic Study	62
4.5	Stability and Reusability of Magnetic Biochar	65
<b>5</b>	<b>CONCLUSIONS AND RECOMMENDATIONS</b>	<b>69</b>
5.1	Conclusions	69
5.2	Recommendations for future work	70
	<b>REFERENCES</b>	<b>71</b>

## LIST OF TABLES

Table 1.1:	Estimated Degree of Fixation for Different Dye/Fibre Combination (Kausar, et al., 2018).	2
Table 1.2:	Common Metal Found in Different Dye Classes (Verma, 2008).	3
Table 1.3:	Characteristics of Dyes (Butler, et al., 2016).	6
Table 1.4:	Advantages and Factors in Selecting Treatment Method for Treating Textile Finishing Wastewater (Pang and Abdullah, 2013).	8
Table 2.1:	Properties of Different Types of Biomass.	15
Table 2.2:	Characteristics of Different Biochar at Various Pyrolysis Temperature.	18
Table 2.3:	Operating Conditions at Different Pyrolysis (Li, et al., 2020b).	20
Table 2.4:	Properties of Hydrochar and Biochar from Manure Waste at Different Temperature (Cárdenas-Aguilar, et al., 2019).	23
Table 2.5:	Oxidation Potential of Common Oxidants (Rosal and Agüera, 2008).	30
Table 4.1:	Summary of Impregnation-Pyrolysis on Production of Magnetic Biochar with Different Feedstock.	46
Table 4.2:	Summary of Chemical Co-Precipitation on Production of Magnetic Biochar with Different Feedstock.	49
Table 4.3:	Summary of Calcination on Production of Magnetic Biochar with Different Feedstock.	51
Table 4.4:	Advantages and Limitations for Each Method (Feng, et al., 2020; Thines, et al., 2017).	52
Table 4.5:	Specific Surface Area and Pore Volume of Different Magnetic Biochar.	56
Table 4.6:	Kinetic Model of Dye Degradation of Modified Magnetic Biochar with AOPs.	64

Table 4.7: Catalytic Effect of Reused Modified Magnetic Biochar Catalysts.

**LIST OF FIGURES**

Figure 1.1: River Water Quality in Malaysia (Huang, et al., 2015).	1
Figure 1.2: World Consumption of Synthetic Dyes (IHS Markit, 2018).	4
Figure 2.1: Annual Biomass Availability in Malaysia (Chan, et al., 2019).	12
Figure 2.2: Schematic Diagram of Interaction Between Functional Group on Biochar and nZVI (Wang, et al., 2019a).	25
Figure 2.3: Graphene Sheet in Forming Single-walled Carbon Nanotubes (Sarkar, et al., 2018).	26
Figure 2.4: Crystal Structure of Different Metal Oxides (Wu, et al., 2015).	29
Figure 2.5: Mechanism for Photocatalytic Activity on the Semiconductor Surface (Zhang, et al., 2018).	32
Figure 4.1: SEM Image of (a-c) Biochar (d) Fe <sub>2</sub> O <sub>3</sub> /TiO <sub>2</sub> Biochar (e) Elemental Mapping (Chen, et al., 2020).	54
Figure 4.2: Dye Removal Mechanism of Fe-impregnated Biochar Catalyst (Rubeena, et al., 2018).	60
Figure 4.3: Mechanism of Methylene Blue Degradation with TiO <sub>2</sub> -Fe <sub>3</sub> O <sub>4</sub> -Biochar Catalyst (Mian, et al., 2019).	62

## LIST OF SYMBOLS / ABBREVIATIONS

$\text{Ag}_3\text{PO}_4$	Silverorthophosphate
$\text{BiOBr}$	bismuth oxybromide
$\text{C}$	carbon atom
$\text{CaCl}_2$	calcium chloride
$\text{CuCl}_2$	cupic chloride
$\text{Cu}^{2+}$	cupric ion
$\text{C/H}$	carbon/hydrogen
$-\text{C}=\text{C}-$	alkene group
$-\text{C}=\text{N}-$	imnie group
$-\text{C}=\text{O}-$	carbonyl group
$-\text{COOH}$	carboxyl group
$\text{CoFe}_2\text{O}_4$	cobalt ferrite
$\text{Co}(\text{NO}_3)_2 \cdot 6\text{H}_2\text{O}$	cobaltous nitrate hexahydrate
$\text{CuFe}_2\text{O}_4$	copper ferrite
$e^-$	electrons
$\text{Fe-CPB}$	iron-coir pith biochar
$\text{Fe-RHB}$	iron-rice husk biochar
$\text{Fe/FBC}$	iron frass-based biochar
$\text{FeCl}_2 \cdot 4\text{H}_2\text{O}$	ferrous chloride tetrahydrate
$\text{FeCl}_3 \cdot 6\text{H}_2\text{O}$	ferric chloride hexahydrate
$\text{Fe}(\text{NO}_3)_3 \cdot 9\text{H}_2\text{O}$	iron (III) nitrate nonahydrate
$\text{FeSO}_4 \cdot 6\text{H}_2\text{O}$	ferrohexahydrate
$\text{FeSO}_4 \cdot 7\text{H}_2\text{O}$	iron (II) sulfate heptahydrate
$\text{FeCl}_3$	iron (III) chloride
$\text{Fe}_3\text{O}_4$	iron oxide
$\text{Fe}_3\text{O}_4$	magnetite
$\text{Fe}_2\text{O}_3$	maghemite, hematite
$\text{Fe}_2\text{O}_3$	iron (III) oxide
$\text{FeSO}_4$	iron sulfate
$\text{Fe}^{2+}$	ferrous ion
$\text{Fe}^{3+}$	ferric ion
$\text{h}^+$	holes

$\text{HO}_2^\bullet$	hydroperoxyl radical
H	hydrogen atom
$\text{H}^+$	hydrogen ion
HCl	hydrochloric acid
$\text{H}_2\text{O}_2$	hydrogen peroxide
H/C	hydrogen/carbon
KOH	potassium hydroxide
$\text{MgCl}_2$	magnesium chloride
MgO	magnesium oxide
nZVI	nano-zerovalent iron
N	nitrogen atom
NaOH	sodium hydroxide
$\text{Na}_2\text{HPO}_4 \cdot 12\text{H}_2\text{O}$	sodium phosphate dibasic dodecahydrate
-N=N-	azo group
-N=O	nitroso group
-NO <sub>2</sub>	nitro group
-NH <sub>2</sub>	amino group
-NR <sub>2</sub>	amino group
O	oxygen atom
O/C	oxygen/carbon
$\text{O}_2^-$	superoxide anion
•OH	hydroxyl radicals
$\text{OH}^-$	hydroxyl ion
-OH	hydroxyl group
$\text{O}_2\text{H}^\bullet$	perhydroxyl radicals
$\text{PO}_4^{2-}$	phosphate ion
$\text{SO}_4^\bullet$	sulfate radical
$\text{Ti}(\text{SO}_4)_2$	titanium disulfate
$\text{Ti}(\text{OBu})_4$	titanium butoxide
$\text{TiO}_2$	titanium dioxide
ZnO	zinc oxide
ZVI	zero-valent iron
AOPs	advances oxidation processes

BET	brunauer-emmett-teller analysis
CEC	cation exchange capacity
EDX	energy dispersive X-ray
FTIR	fourier-transform infrared spectroscopy
PAH	polycyclic aromatic hydrocarbons
PMS	peroxymonosulfate
PDS	peroxydisulfate
SEM	scanning electron microscopy
XPS	X-Ray photoelectron spectroscopy
XRD	X-ray diffraction

## CHAPTER 1

### INTRODUCTION

#### 1.1 Water Pollution in Malaysia

Water pollution is defined as water that is contaminated by harmful substances and resulting in a negative impact on the quality of water. Human activities, discharge of industrial effluent wastes and agricultural practices are the major causes of water pollution.

Generally, the polluted sources can be divided into point and non-point sources. For example, point sources are industrial and municipal wastewater which originated from a specific point that can be identified such as a wastewater treatment plant (Huang, et al., 2015). Meanwhile, non-point sources are sources that come from different sources instead of a single source.

The maintenance of good river water quality is important as there are about 97 % of the water supply in Malaysia comes from the river (Chan, 2012). Figure 1.1 illustrates the quality of water in the river from 2005 to 2012. The number of clean rivers started to decrease from 2007 to 2011 whereas the slightly polluted river also decreased from 2009 to 2011 and slightly increased in 2012. Besides, the polluted river number was decreased from 2010 to 2012. The decrease of the number of slightly polluted and polluted river was due to the stringent environmental regulations imposed by the government.

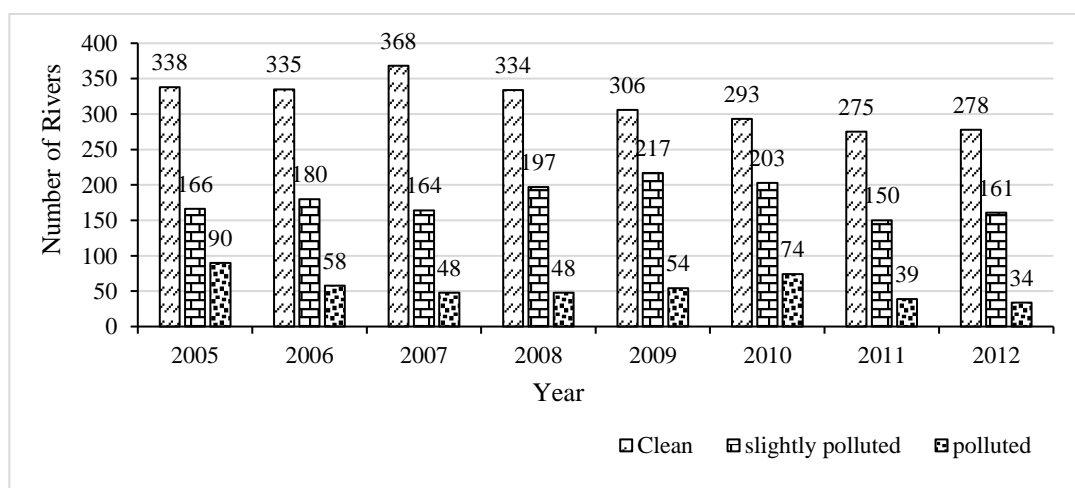


Figure 1.1: River Water Quality in Malaysia (Huang, et al., 2015).

## 1.2 Textile Industry and Environmental Impact

The textile industry involves the processing of raw materials into fabrics and other products (Prazeres, et al., 2014). Raw materials used in the textile industry are divided into two different types such as natural fiber and synthetic fiber. Wool, silk and cotton are examples of natural fiber whereas polyester, viscose and polyamide are examples of synthetic fiber (Madhav, et al., 2018). Besides, the textile industry is one of the top industries that turns a large amount of fresh water into wastewater and caused negative impact to the environment (Dos Santos, et al., 2018).

The textile industry that produces wastewater is characterised by parameters such as chemical oxygen demand, pH, colour, biochemical oxygen demand and salinity (Dos Santos, et al., 2018). The parameters vary depends on dye characteristics. The effluents are mostly comprised of dyes, inorganic and organic pollutants. Those effluents are carcinogenic, toxic and mutagenic to living organisms. Moreover, there are tons of dyes discharged to the effluent during the dyeing process due to improper dyeing process (Kausar, et al., 2018). Table 1.1 shows the estimated degree of fixation for different dye classes of fibre. Based on Table 1.1, there are a certain amount of dyes being a loss to the environment since dyes are not completely fixed to the textile product. Thus, the loss of effluent might cause a serious impact on the environment.

Table 1.1: Estimated Degree of Fixation for Different Dye/Fibre Combination (Kausar, et al., 2018).

<b>Dye class</b>	<b>Fibre</b>	<b>Degree of fixation (%)</b>	<b>Loss to effluent (%)</b>
Acid	Polyamide	80-95	5-20
Basic	Acrylic	95-100	0-5
Direct	Cellulose	70-95	5-30
Disperse	Polyester	90-100	0-10
Metal-complex	Wool	90-98	2-10
Reactive	Cellulose	50-90	10-50
Sulphur	Cellulose	60-90	10-40
Vat	Cellulose	80-95	5-20

In addition, discharge of dye brought negative impact to the environment. The presence of dyes in water bodies threaten marine life due to the existence of aromatics compounds and metals. For instance, heavy metals such as chromium, manganese, zinc, nickel, and copper associated with a dye that is discharged into wastewater and soil might increase the risk of human health and the environment. Table 1.2 depicts the summary for common heavy metals that are found in different dye classes. Heavy metals that are discharged associated with dyes with toxicity properties are mutagenic, carcinogenic and genotoxic had been causing a negative effect on the aquatic ecosystem and human health (Hameed and El-Khaiary, 2008).

Table 1.2: Common Metal Found in Different Dye Classes (Verma, 2008).

<b>Dye classes</b>	<b>Metals in dyes</b>
Acid	Copper, lead, zinc, chromium, cobalt
Basic	Copper, zinc, lead, chromium
Direct	Copper, lead, zinc, chromium
Mordant	Chromium
Pre-metallized	Cobalt, chromium, copper
Reactive	Copper, chromium, lead
Vat	None
Disperse	None

Not only that, dyes also reduce the penetration of sunlight into the water due to the non-biodegradable nature of the organic dye and the high colour intensity (Madhav, et al., 2018). This also results in a decrease in dissolved oxygen level. Fish and other aquatic life are threatened when the dissolved oxygen level is dropping. Besides, lung, skin irritations, headache and nausea are also the effects of exposure to certain dyes. Triphenylmethane dyes such as crystal violet, malachite green and acid violet 19 consist of complex aromatic molecular structure that promotes tumour development in certain species of fish. These dyes are cytotoxic in mammalian cells and phototoxicity in farm crops (Jadhav, et al., 2012).

### 1.3 Production and Classifications of Dyes

Dyes are coloured substances that are soluble in water. Dyes provide the important insight that most of the industries such as textile, paper cosmetic, rubber and others used to impart colours to various substances from the past until today. Today, it is estimated that more than  $1 \times 10^5$  dyes are commercially available with over  $7 \times 10^5$  dyes are produced annually worldwide (Robinson, et al., 2004). Figure 1.2 shows that China is the major consumer which has consumed over 43 % of world's synthetic dyes capacity (IHS Markit, 2018). This is because China has the largest population, hence, leading to a large consumption in the textile manufacturer.

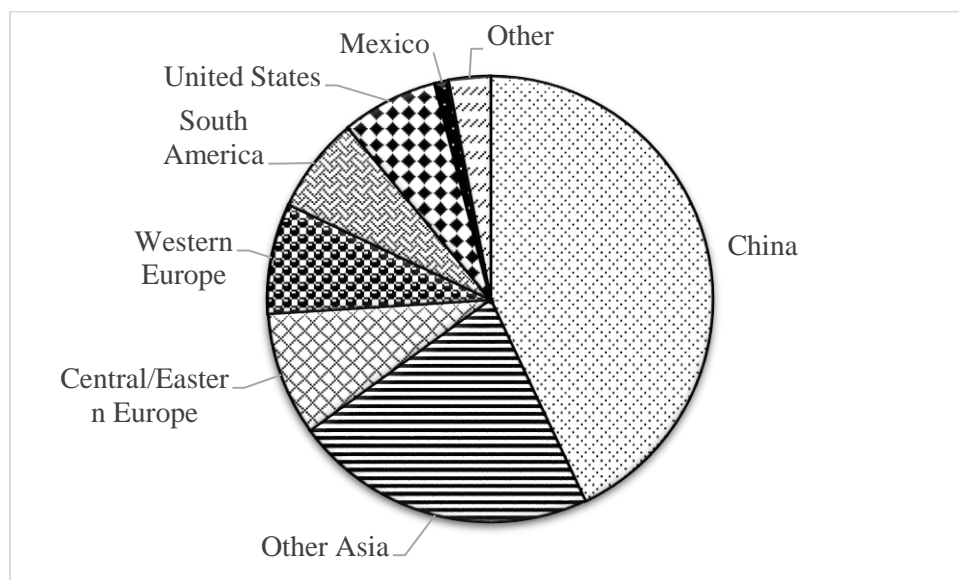


Figure 1.2: World Consumption of Synthetic Dyes (IHS Markit, 2018).

Dye molecules are coloured organic compounds that can be classified in different ways. There are two main functional groups in dye molecules such as chromophore and auxochrome (Kausar et al., 2018). Chromophore is known as a group of atoms which normally an electron-withdrawing group that controls the dye colour whereas auxochrome is known as an electron-donating substituent that increase the intensity colour of the chromophore. The examples of chromophore group are  $-C=C-$ ,  $-C=N-$ ,  $-C=O-$ ,  $-N=N-$ ,  $-N=O$ ,  $-NO_2$ . A few common examples for auxochrome group are  $-NH_2$ ,  $-NR_2$ ,  $-COOH$ , and  $-OH$  groups (Pang and Abdullah, 2013).

Besides, dyes can be classified as direct, basic, disperse, vat, reactive, sulfur, and acid dyes as illustrated in Table 1.3. Acid dyes are water-soluble anionic compounds. There are few examples of acid dyes such as naphthol yellow, martius yellow and methyl orange which normally applicable for wool, nylon and others. Acid dyes are divided into azo dyes, triarylmethane dyes, and anthraquinone dyes (Butler, et al., 2016). Azo dyes comprise of carbon atoms with two adjacent nitrogen atoms. Azo dye is one of the largest production of dyes which amounted to 70 % of the total dyes produced (Pang and Abdullah, 2013).

For basic dyes, they are water-soluble that normally applied from an acidic dye bath and suitable for some polyesters and acrylic. Malachite green, crystal violet and basic yellow 28 are examples of basic dyes. On the other hand, direct dyes are also water-soluble and anionic compounds that can be used directly to cellulosic without the presence of mordants such as copper and chromium. Copper and chromium act as mordants that help to enhance the fastness of dyes on fibres. Examples of direct dyes include direct orange 26, direct black and direct blue. Disperse dyes such as disperse yellow 3, disperse blue 27 and disperse red 4 have a very low water solubility which fibres usually applied to acetate, polyester and other synthetics.

Furthermore, reactive dyes are the next group of dyes that need to be highlighted. Reactive dyes are accessible to cotton, wool and other cellulosic. For instance, reactive blue 5, reactive red and reactive yellow are dyes that have characteristics of water-soluble and anionic compounds. Reactive dyes have the lowest degree of fixation on fibre which approximately 50 % remains in wastewater due to their inefficient dyeing process (Lau and Ismail, 2009).

Another type of dye is a sulfur dye that contains sulfur or sodium sulphide. Sulfur dye is normally applied to fibre such as cotton and other cellulosic. Lastly, vat dyes such as vat green 6, indigo and vat blue are water insoluble and known as the oldest dyes among all (Kausar, et al., 2018). In short, different classes of dyes have different characteristics and its fibres applied vary. Table 1.3 summarizes all dye classes with their characteristics respectively.

Table 1.3: Characteristics of Dyes (Butler, et al., 2016).

<b>Dye classes</b>	<b>Description</b>	<b>Fibres typically applied to</b>	<b>Typical pollutants associated with various dyes</b>
Acid	Water-soluble anionic compounds	Wool, nylon	Colour; organic acids; unfixed dyes
Basic	Water-soluble, applied in weakly acidic dye baths; very bright dyes	Acrylic, some polyesters	N/A
Direct	Water-soluble, anionic compounds; can be applied directly to cellulosic without mordant's (or metals like chromium and copper)	Cotton, rayon, other cellulosic	Colour; salt; unfixed dye; cationic fixing agents; surfactant; defoamer; levelling and retarding agents; finish; diluents
Disperse	Not water-soluble	Polyester, acetate, other synthetics	Colour; organic acids; carriers; levelling agents; phosphates; defoamers; lubricants; dispersants; delustrants; diluents
Reactive	Water-soluble, anionic compounds; largest dye class	Cotton, other cellulosic, wool	Colour; salt; alkali; unfixed dye; surfactants; defoamer; diluents; finish
Sulfur	Organic compounds containing sulfur or sodium sulphide	Cotton, other cellulosic	Colour; alkali; oxidising agent; reducing agent; unfixed dye
Vat	Water-insoluble; oldest dyes; more chemically complex	Cotton	Colour; alkali; oxidising agents; reducing agents

#### 1.4 Removal Techniques

In industry, numerous treatment methods have been investigated to treat wastewater due to the presence of organic dyes in the wastewater effluent. Physical methods, chemical methods, and biological methods are the three main types of treatment methods that are used to treat textile wastewater. Nevertheless, each method has its advantages and drawbacks that need to be addressed. Table 1.4 shows the advantages and limitations that need to be taken into considerations for different treatment methods.

Based on Table 1.4, the physical method for wastewater treatment includes ion exchange, adsorption and membrane filtration process. The ion exchange process is a technique that removes undesirable anions and cations from wastewater. The exchange of ions in wastewater to form strong bonds between resins and solute can help in removing dyes (Ahmad, et al., 2015). The process starts when the water flowing through the base until it becomes saturated. Then, it involves the regeneration through backwashing the resin in removing accumulated solids. Only basic dyes, acid dyes, direct dyes and reactive dyes can be effectively removed since those dyes possess a characteristic of anionic or cationic (Pang and Abdullah, 2013). Ion exchange treatment method can remove soluble dyes effectively but show poor removal results in non-ionic dyes.

On the other hand, adsorption is one of the techniques in removing the dye molecule which involves collecting soluble substances in the solution on an appropriate interface (Rangabhashiyam, Anu and Selvaraju, 2013). Dye molecules are adsorbed on the surface of an adsorbent through van der Waals forces, electrostatic forces or hydrogen bonding. Activated carbons have been used as an adsorbent since they can adsorb various dyes with better adsorption capacity. However, it is expensive because activated carbon regeneration is needed. Therefore, some researchers have investigated the removal of dyes using different types of low-cost adsorbents such as castor bean, milled sugarcane bagasse, corn cobs in recent years (Ahmad, et al., 2015).

Table 1.4: Advantages and Factors in Selecting Treatment Method for Treating Textile Finishing Wastewater (Pang and Abdullah, 2013).

Treatment methods	Advantages	Factors to be considered
<b>Physical method</b>	- Efficient removal for various types of dyes.	- Need regeneration or disposal absorbent.
- Adsorption	- No loss of adsorbent during regeneration.	- Not effective for all types of dyes.
- Ion exchange	- Efficient removal for all types of dye	- Concentrated sludge production, running cost
- Membrane filtration		- Incapable of treating large volumes.
<b>Biological method</b>	- Efficient removal for azo dyes. Lower operating cost and sludge can be recycled.	- Longer detention times, large land are required and sensitivity to toxic organic dye.
- Aerobic process	- Lower operating cost and biogas produced can be used as fuel source.	- Longer residence time to reproduce the cell, sensitivity to toxic organic dye and production of aromatic amine.
- Anaerobic process		
<b>Chemical method</b>	- Short detention time and high removal efficiencies for various types of dyes.	- High cost of chemical reagent and pH adjustment.
- Chemical coagulation and flocculation		- High production sludge, handling and disposal problems.
<b>Chemical oxidation</b>	- Efficient removal for various types of dyes in a short time	- Costly chemical reagent, high sludge production, handling and disposal problems.
- Fenton oxidation	- Efficient removal for various types of dyes.	- Not suitable for dispersed dyes. Short half-life (20 mins)
- Ozonation	- No production of sludge	- Relatively new methods. Formation of by-products.
- Photocatalytic or sonocatalytic oxidation		- Penetrability of ultraviolet light in water medium is often less.

For membrane filtration process, it is an advanced technology applied after coagulation and flocculation. Several filtration technologies such as nanofiltration, ultrafiltration, microfiltration, and reverse osmosis are used for wastewater treatment. Filtration is the process of passing wastewater through membranes with small pores. It can help in separating two or more components from liquid streams by their molecular size. Table 1.4 depicts a few limitations experienced by filtration such as concentrated sludge is produced during the filtration process, which leads to frequent cleaning and replacement of modules is needed. The filtration process also requires high capital costs.

Furthermore, biological treatment is the process of utilizing microorganisms under anaerobic or aerobic conditions to remove the contaminants of wastewater. Anaerobic wastewater treatment is the process that microorganisms degrade those organic contaminants in the absence of oxygen. The advantages of using biological treatments are low operating cost, and the methane gas produced from the process can be used as a fuel source as stated in Table 1.4. However, dyes degradation by microorganisms might lead to the creation of aromatic amines when azoreductase cleavage of the azo bond (Haroun and Idris, 2009). Besides, it is not feasible for the last step treatment because it's only a partial degradation treatment and long acclimatization time is required for the growth of microorganisms (Pang and Abdullah, 2013).

For aerobic conditions, it is not effective for treating textile wastewater since azo dyes cannot be removed significantly. Low biodegradability index (5 days of biological oxygen demand/chemical oxygen demand  $< 0.1$ ) of azo dyes is the factor that resistant to conventional biological treatment (Baban, et al., 2010). There are also few disadvantages in aerobic biological processes such as longer hydraulic retention time is required, unknown oxidation compounds are formed that intensifies the colour of wastewater, and undesirable flocs formations which cause the ineffectiveness of organic dyes biodegradation (Pang and Abdullah, 2013).

Coagulation or flocculation process and chemical oxidation process are examples of chemical treatment. The coagulation or flocculation process is adequate for the primary treatment of textile effluents which weaken the colloidal particles by adding coagulants. This process normally led to the large

production of toxic sludge and caused disposal problems. For the chemical oxidation process, chemical reagents such as catalysts and oxidizing agents are used for the reaction.

### **1.5 Problem Statement**

Water pollution is a common issue over the years as wastewater is not treated properly. The increase of polluted rivers had caused the increase of people suffering from water-related diseases. Since the world population increased every year, the demand for textile manufactured also increased due to the improving sense of lifestyle. This had brought a negative impact on the environment due to the discharge of organic dyes from textile industries. Dye effluents are hard to degrade due to their ability to withstand aerobic digestion, stability under light, oxidising agents and heat (Rangabhashiyam, Anu and Selvaraju, 2013).

Generally, the conventional methods for the removal of organic dyes are inefficient and expensive. Conventional methods such as chemical precipitation requires large amount of chemicals in reducing the concentration of dyes to meet the standard requirement before discharging to environment (Barakat, 2011). Besides, high sludge production, poor settling, slow metal precipitation, handling and disposal problems would create a long-term environmental impact (Barakat, 2011). Thus, it is important to develop environmentally sustainable methods to treat the organic dyes effluent prior to discharge. The adsorption process is more preferable due to its high efficiency and simplicity in operation.

However, large amount of adsorbent wastes are produced after the removal of organic dyes. The increasingly produced waste will give rise to secondary pollution. Therefore, managing waste is important to reduce the effect of waste on health and the environment. For instance, recycling and planning the waste management is a challenging task which involves understanding and scientific knowledge to ensure the effectiveness of the process. Magnetic biochar is known as a cost-effective adsorbent that can degrade organic contaminants effectively and can be easily recycled through magnetic separation. It is essential to evaluate the reusability and stability of

modified magnetic biochar which can subsequently reduce the operation cost and generation of wastes.

### **1.6 Aim and Objectives**

The main purpose of this study is to investigate the application of modified magnetic biochar for the degradation of organic dyes using advanced oxidation processes. The sub-objectives include:

- (i) To investigate different synthesis methods in producing modified magnetic biochar for the removal of organic dyes in wastewater.
- (ii) To review the characteristic of different modified magnetic biochar for the degradation of organic dyes in wastewater.
- (iii) To evaluate the reusability and stability of magnetic biochar catalysts.

## CHAPTER 2

### LITERATURE REVIEW

#### 2.1 Biochar

Biochar is a solid that is rich in carbon and also a form of carbonaceous material which is produced from biomass (Weber and Quicker, 2018). Biomass is known as a renewable source. It is composed of organic matters such as plant residues, agricultural wastes, animal manures, and wood. Chan, et al., (2019) stated that Malaysia is a country that is rich in biomass due to its suitable climate for agricultural activities and also has dense tropical rainforest for the timber industry. These also lead to large amount of wastes being produced every year. Figure 2.1 shows the annual biomass availability in Malaysia. Based on Figure 2.1, palm oil trees were the highest portion as compared to other biomass and also found that the production of palm waste was increasing over the years. Thus, effective ways should be done by utilizing these wastes as biochar's feedstock in various applications instead of disposing them.

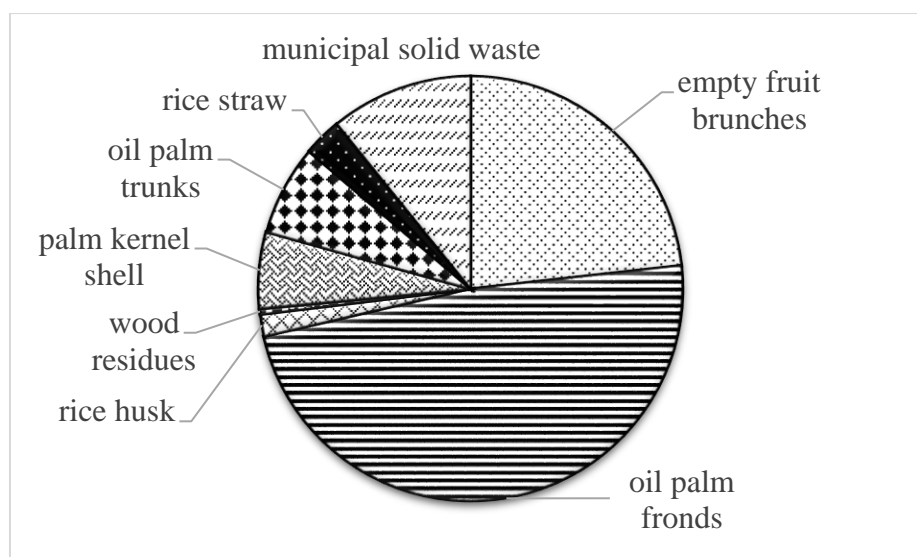


Figure 2.1: Annual Biomass Availability in Malaysia (Chan, et al., 2019).

The major element of biochar is carbon while the remaining elements include oxygen, hydrogen, ash, and trace amount of inorganics such as sulphur

and nitrogen. However, the elemental compositions for biochar are different based on their production and source of biomass (Cha, et al., 2016). Biochar possesses unique properties and characteristics such as large surface area, high cation exchange capacity, porous structure, and abundant oxygen-containing functional groups (Eltaweil, et al., 2020). It is also inexpensive and environmentally friendly. Moreover, biochar has several advantages such as the fast and easy preparation, cost-effectiveness, and reusability that gained attention towards some researchers (Yaashikaa, et al., 2020).

Recently, biochar has been extensively applied in various applications such as fuel cell, supercapacitor, energy conversion, and storage as well as catalyst support (Shan, et al., 2020). Biochar is also similar to activated carbon. It is also widely used as adsorbent to remove organic and inorganic pollutants such as heavy metals, dyes, phenols, chemical intermediate, and others (Godwin, et al., 2019). It has been proved that biochar can remove dyes effectively. In the study of the removal of methylene blue dye using cow dung biochar, it was found that 99 % of removal efficiency was achieved (Ahmad, et al., 2020). Besides, the adsorption efficiency of biochar also depends on the raw biomass material used for the production of biochar. Ahmad, et al., (2020) evaluated that cow dung was the most effective biochar among rice husk, cow dung, and sewage as it was able to degrade 99 % of the methylene blue dye in synthetic wastewater. This showed that the nature of raw materials plays an important role in degrading contaminants (Zhang, et al., 2018a). Characteristics such as large surface area, porous structure, and functional groups of surface brought biochar as a good adsorbent material (Pereira Lopes and Astruc, 2021).

Besides adsorbing organic and inorganic pollutants, biochar also helps in boosting crop growth. Zhang, et al., (2018a) reported that the usage of biochar as the carrier of fertilizer in the soil had been used frequently nowadays to reduce fertilizer loss subsequently promote crop growth and improve the soil environment. Moreover, biochar itself has mineral nutrients such as potassium, calcium, magnesium, and nitrogen which provide nutrients to the crop directly. The porous structure of biochar also allows microorganisms to have a better habitat environment that increases the yield (Zhang, et al., 2018a).

## 2.2 Feedstocks of Biochar

Many organic wastes can be used as feedstocks to produce biochar since biochar is derived from biomass. Biomass can be divided into two categories which are woody and non-woody biomass. For instance, woody biomass consists of residues from forestry and trees whereas non-woody biomass comprises industrial wastes, crops, and animal manures (Tomczyk, Sokołowska and Boguta, 2020). Woody biomass is characterised by high bulk density, low moisture, low ash, and high calorific value. Conversely, non-woody biomass is characterised by low bulk density, high moisture content, high ash, and low calorific value (Jafri, et al., 2018). The higher moisture content of biomass leads to lower maximum combustion temperature, thermal efficiency, and increase the pollutant emissions (Liu and Han, 2015).

Biomass comprises three main organic components which are lignin, cellulose, and hemicellulose. The volatile content matter and heating values depend on the amount of lignin, cellulose, and hemicellulose (Jafri, et al., 2018). Table 2.1 shows the properties of various types of biomass for the production of biochar. It was observed that different biomass contains different amounts of volatile matter, fixed carbon, ash content, carbon, hydrogen, nitrogen, and oxygen. The properties of each biomass feedstock play an important role in the thermal conversion process as it affects the ash content, carbon content, and carbon sequestration capacity of biochar (Pandey, Daverey and Arunachalam, 2020). Based on Table 2.1, the ash content for rice husk was 14.02 % which was 8.62 % higher than sugarcane bagasse. Similar studies also reported by El-gamal, et al., (2017) that the ash content and lignin of rice husk biomass were higher than sugarcane bagasse. In contrast, the content of cellulose and hemicellulose of sugarcane bagasse was higher than rice husk.

Besides, it was observed that woody biomass such as oak sawdust, pine sawdust, and pinewood had lower ash content compared to non-woody biomass. To illustrate, Keiluweit, et al., (2010) found that the ash content for wood biochar was 1.2 % whereas the grass biochar was 6.9 %. This is because woody biomass has higher cellulose, hemicellulose, and lignin content than grass biomass.

Table 2.1: Properties of Different Types of Biomass.

Biomass	Proximate analysis (%)			Ultimate analysis (%)				References
	Volatile matter	Fixed carbon	Ash	C	H	N	O	
Oak sawdust	69.24	16.51	0.81	52.28	5.74	0.06	41.92	(Zhang, et al., 2012)
Pine sawdust	83.10	16.80	0.10	51.00	6.00	0.10	42.90	(Luo, et al., 2015)
Pinewood	85.45	13.15	1.40	48.15	6.70	1.35	43.60	(Liu and Han, 2015)
Coconut fibre	80.85	11.10	8.05	47.75	5.61	0.90	45.51	(Liu and Han, 2015)
Corn cob	69.50	15.90	2.90	48.12	6.48	-	43.51	(Liu, et al., 2014)
Palm kernel shell	66.80	17.90	3.40	55.82	5.62	0.84	37.73	(Lee, et al., 2013)
Paddy straw	56.40	15.40	20.90	48.75	5.98	1.99	43.28	(Lee, et al., 2013)
Rice husk	54.39	23.71	14.02	44.13	5.01	0.39	50.40	(Danish, et al., 2015)
Sugarcane bagasse	74.30	20.30	5.40	45.40	6.70	0.90	46.90	(Luo, et al., 2015)
Tea wastes	70.29	18.57	3.88	48.60	5.43	3.80	42.17	(Uzun, et al., 2010)
Almond shell	74.90	21.80	3.30	50.30	6.20	1.00	42.50	(Elleuch, et al., 2013)

Moreover, cation exchange capacity, pH, and specific surface area of biochar are dependent on the type of feedstock of biomass and pyrolysis temperature. The cation exchange capacity (CEC) of biochar derived from paper mill waste was lower than biochar derived from sugarcane bagasse. Experiments conducted showed that the CEC for paper mill waste was about 9 to 18 cmol/kg whereas the CEC for sugarcane bagasse was 122 cmol/kg (Van Zwieten, et al., 2010; Carrier, et al., 2012). This is because the higher ash content of biomass can produce a higher CEC value of biochar (Tomczyk, Sokołowska and Boguta, 2020). Another reason might also be due to the enhancement of forming oxygen-containing functional groups by the alkali and alkali metals in biomass. Several researchers also revealed that the CEC of chicken manure-derived biochar was higher than the pig manure-derived biochar at 500 °C (Cely, et al., 2015). This also further proved that the value of CEC varies with the feedstock of biomass.

Specific surface area is also one of the significant properties of biochar. El-gamal, et al., (2017) reported that the biochar derived from sugarcane bagasse had a larger specific surface area and pore size than the rice husk biochar. It was observed that the specific surface area for sugarcane biochar was 185.6 m<sup>2</sup>/g while rice husk was 154.7 m<sup>2</sup>/g. At the same time, pyrolysis temperature also affects the specific surface area and pore volume of the biochar. The specific surface area for sugarcane and rice husk biochar at 450 °C were 107.87 m<sup>2</sup>/g and 98.01 m<sup>2</sup>/g, respectively. The values were increased to 124.11 m<sup>2</sup>/g and 212.99 m<sup>2</sup>/g at 550 °C, respectively (El-gamal, et al., 2017). To further illustrate this, the higher the pyrolysis temperature, the larger the specific surface area. This was attributed to the forming of the micropore structures. During pyrolysis, the surface area increased due to the formation of channel structures and decomposition of organic components in the biomass (Tomczyk, Sokołowska and Boguta, 2020).

As mentioned earlier, the pH of the biochar also depends on the feedstock of the biochar. Tomczyk, Sokołowska and Boguta, (2020) illustrated that the pH for the application of biochar was normally fall in the range of 7.1 to 10.5. For instance, the pH for the biochar-derived corn straw, soybean straw, and peanut straw were 9.3, 7.6, and 8.6 respectively at the pyrolysis temperature of 300 °C (Yuan, Xu and Zhang, 2011). Biochar's pH not only

varies with the feedstock of biomass but also changes depending on the pyrolysis temperature. At 500 °C, biochar derived canola straw, corn straw, soybean straw, and peanut straw were found at the pH of 9.3, 10.7, 10.9, and 10.8, respectively. Meanwhile, the pH values were at 10.7, 11.3, 11.2, and 11.2, respectively when the pyrolysis temperature increased to 700 °C (Yuan, Xu and Zhang, 2011). Furthermore, the pH of the biochar might also be correlated to the organic components of biomass such as lignin, hemicellulose, and cellulose.

In short, pH, CEC, and specific surface area of biochar are highly affected by the pyrolysis temperature. Table 2.2 summarizes the characteristics of different feedstock biochar at various pyrolysis temperatures. Tomczyk, Sokołowska and Boguta, (2020) illustrated that an increase in temperature will increase the specific surface area of biochar. This statement can be proved as the specific surface area of the biochar rice husk derived increases from 32.70 m<sup>2</sup>/g to 261.71 m<sup>2</sup>/g when the pyrolysis temperature increases from 350 °C to 650 °C (Claoston, et al., 2014). Similar studies also reported by Ding, et al., (2014) that the specific surface area of sugarcane bagasse biochar derived increased from 0.78 m<sup>2</sup>/g to 14.1 m<sup>2</sup>/g at the temperature of 400 °C to 600 °C. The specific surface area of biochar increases most likely due to the thermally cracked in the pore-blocking substance. Moreover, higher pyrolysis temperature also promotes the formation of pores and releases of volatile matter.

According to Table 2.2, it was observed that the pH of empty fruit bunch of biochar derived increased from 8.3 to 10.2 during an increase in the pyrolysis temperature. Ding, et al., (2014) mentioned that the pH of biochar is correlated in creating carbonate compounds and the contents of inorganic alkalis. This provides a clear evidence that an increase in temperature also increases the content of total base cations and carbonates. Consequently, it contributes to an increase in pH value (Tomczyk, Sokołowska and Boguta, 2020). However, the results revealed by Zama, et al., (2017) were opposed to the previous claim as the pH of peanut shell biochar decreased from 11.1 to 10.6 when the temperature increased from 440 °C to 500 °C. This was probably due to the highest ash content in peanut shell biochar at 440 °C (Zhao, Ta and Wang, 2017).

Table 2.2: Characteristics of Different Biochar at Various Pyrolysis Temperature.

<b>Biochar feedstock</b>	<b>Pyrolysis temperature (°C)</b>	<b>Specific surface area (m<sup>2</sup>/g)</b>	<b>pH</b>	<b>CEC (cmol/kg)</b>	<b>References</b>
Rice husk	350	32.70	6.6	10.8	
	500	230.91	7.9	9.3	(Claoston, et al., 2014)
	650	261.71	8.8	8.3	
Empty fruit bunch	350	11.76	8.3	21.5	
	500	15.42	9.8	14.6	(Claoston, et al., 2014)
	650	28.20	10.2	12.0	
Sugarcane bagasse	400	0.78	6.9	3.8	
	500	1.98	7.3	9.6	(Ding, et al., 2014)
	600	14.1	7.6	4.1	
Peanut shell	350	14.03	10.4	26.5	
	440	14.08	11.1	23.7	(Zama, et al., 2017)
	550	18.58	10.6	19.7	

The CEC content varies with various kinds of biochar feedstock at different pyrolysis temperatures. The CEC content for empty fruit bunch derived biochar decreased from 21.5 cmol/kg to 12.0 cmol/kg when the pyrolysis temperature increased from 350 °C to 650 °C (Claoston, et al., 2014). This was because some of the functional groups had been removed and aromatic carbon had been formed during the heating process (Tomczyk, Sokołowska and Boguta, 2020). Several researchers reported that the CEC content of the biochar decreased when the pyrolysis temperature increased (Zama, et al., 2017; Claoston, et al., 2014). Banik, et al., (2018) also mentioned that the distribution of oxygen-containing functional groups on the surface of biochar also correlated with the CEC of biochar.

### **2.3 Production of Biochar**

Biochar can be produced through thermochemical decomposition methods that involve high temperature which is derived from biomass. Most of the common methods that are employed in producing biochar are pyrolysis, gasification, and hydrothermal carbonization.

#### **2.3.1 Pyrolysis**

Pyrolysis is the most widely used technique in producing carbon-rich biochar which is the process of decomposing organic materials thermally at the temperature of 300 °C to 900 °C with limited oxygen available (Cha, et al., 2016). The pyrolysis process involves the reaction of fragmentation, cross-linking and depolymerization in producing syngas, bio-oil and biochar which relates to cellulose, hemicellulose and lignin of biomass. Normally, the pyrolysis process is more preferable for biomass with lower moisture content (Nidheesh, et al., 2020). Pyrolysis can be divided into slow pyrolysis, fast pyrolysis and flash pyrolysis by categorizing them based on the residence time, pyrolysis temperature and heating rate (Li, et al., 2020b).

Table 2.3 summarizes the operating conditions during different pyrolysis. Among slow pyrolysis, fast pyrolysis and flash pyrolysis, slow pyrolysis is most frequently used as it can produce more yield. Slow pyrolysis is also the most feasible process in the production of biochar. This is because the residence time is longer and it has a lower heating rate for slow pyrolysis

(Nidheesh, et al., 2020). After the pyrolysis process, the by-products formed such as biogas and bio-oil can be used for gas turbines and engine purposes. For fast pyrolysis, the process mostly involves a small size of biomass in the heating within the temperature of 850 K to 1250 K at a residence time around 0.5 s to 1.0 s. Only a small amount of biochar was produced for a fast pyrolysis process with large amount of by-products such as bio-oil and biogas. High heating rate and low residence time are some of the contributing factors to avoid secondary reactions. Therefore, fast pyrolysis is more suitable in producing liquid products with high yield with its operating conditions (Cha, et al., 2016). Besides, flash pyrolysis is the process that the biomass is heated under the temperature of 1050 K to 1300 K with the flash residence time less than 0.5 s. Xiang, et al., (2020) also reported that the yield of biochar decreased when the residence time is prolonged and the decomposition for biomass will be more complete.

Table 2.3: Operating Conditions at Different Pyrolysis (Li, et al., 2020b).

<b>Condition</b>	<b>Residence time (s)</b>	<b>Pyrolysis temperature (K)</b>	<b>Heating rate (K/s)</b>
<b>Slow pyrolysis</b>	450-550	550-950	0.1-10
<b>Fast pyrolysis</b>	0.5-1.0	850-1250	10-200
<b>Flash pyrolysis</b>	<0.5	1050-1300	<1000

### 2.3.2 Gasification

The gasification process is the heating process converting biomass to syngas and biochar in partial oxidation conditions (You, et al., 2017). Gaseous products such as carbon monoxide, carbon dioxide, hydrogen, nitrogen, and others are formed by reacting the carbonaceous contents of feedstock in air, steam and mixture at a temperature higher than 800 °C. Solid products such as biochar, ash, tar and oil are also produced.

The process of gasification only involves heating at a high temperature which presents that the required temperature is higher than the pyrolysis process. High levels of alkali salts and alkaline earth minerals are found in the production of biochar through the gasification process (Xiang, et al., 2020). Besides, harmful substances such as total polycyclic aromatic hydrocarbons

(PAHs) were also formed in the presence of high temperature and oxygen (Rollinson, 2016). The PAHs that exist on the surface of biochar provide a larger surface area and micropores volume. Generally, the specific surface area and pore volume of produced biochar are smaller compared to slow and fast pyrolysis processes because of the high temperature employed causing the effect of pore clogging, pore expansion and tar deposition (You, et al., 2017). Similar to the pyrolysis process, the characteristics of biochar for gasification are also affected by residence time, temperature and heating rate. You, et al., (2017) illustrated that the yield of biochar for the gasification process was lesser than other thermochemical processes because of its partial oxidation process.

In addition, the carbon content in biochar decreased during the gasification process. It is possible to speculate that the carbon content decreased because of its conversion from carbon to gaseous compounds such as carbon monoxide and carbon dioxide with its high severity (Azargohar, et al., 2019). Besides, the atomic ratio of hydrogen/carbon (H/C) and oxygen/carbon (O/C) also decreased when the gasification temperature increased due to its enhancement of aromatic structures of biochar. For instance, the carbon and hydrogen content for canola meal-derived biochar was 48.9 % and 4.9 % at 650 °C and decreased to 47.6 % and 4.1 % at 750 °C in the gasification process (Azargohar, et al., 2019). There was a significant loss in functional groups such as carbonyl, carboxyl, and hydroxyl groups due to the high temperature in the gasification process (You, et al., 2017). These resulted in fewer functional groups for biochar compared to biochar that was produced through pyrolysis or hydrothermal carbonization process. Higher ash content and pH value were also found in the biochar through the gasification process (Hansen, et al., 2015).

Although the gasification process produced the least amount of biochar, the involved cost of production was low with a high yield of syngas. A large amount of energy per unit mass of carbonaceous materials was produced because of the higher efficiency in the conversion of carbon than slow and fast pyrolysis. Not only that, the production of heat and electricity could be used in biochar related downstream treatment systems to improve the economic feasibility of gasification systems (You, et al., 2017).

### 2.3.3 Hydrothermal Carbonization

Hydrothermal carbonization is a process where the wet biomass is heated at a low temperature range of 120 °C to 260 °C and a pressure range of 2 MPa to 10 MPa with limited oxygen conditions (Xiang, et al., 2020). The product formed from hydrothermal carbonization is hydrochar instead of biochar. Besides hydrochar, liquid products such as inorganic salts, organic acids, and sugars and gaseous products such as carbon dioxide are formed. During the hydrothermal carbonization process, most of the carbohydrates decomposed whereas organic compounds such as lignin were degraded to a lesser extent due to the low temperature (Rodriguez Correa, et al., 2019).

Similar to previous studies, the properties of hydrochar such as specific surface area, pore volume, pH, CEC, the functional group on the surface of biochar depend on the temperature, residence time and heating rate (Cárdenas-Aguiar, et al., 2019). Hydrochar exhibits higher hydrogen/carbon (H/C) and C/H ratios than biochar because the formation of an aromatic structure for hydrochar is not as stable as biochar after pyrolysis. Table 2.4 shows the properties of hydrochar and biochar from manure waste at different temperatures. Cárdenas-Aguiar, et al., (2019) reported that the pH value of hydrochar increases with the increasing hydrothermal carbonization temperature. This can be further explained that the produced hydrochar at 240 °C had a higher pH value than hydrochar produced at 190 °C. Some organic acids also tend to form during the hydrothermal carbonization process which favours the organic acid to adsorb on hydrochar (Weber and Quicker, 2018).

The CEC value of hydrochar decreases significantly when the temperature increases. This might be due to the decrease in oxygen-containing functional groups. From Table 2.3, it was observed that the CEC value in hydrothermal carbonization at 190 °C was 39.2 cmol/kg and decreased to 18.9 cmol/kg when hydrothermal carbonization at 240 °C. In addition, the surface area of hydrochar was larger than biochar through pyrolysis with increasing temperature due to the decomposition of cellulose and hemicellulose structures. With the presence of water at low temperature in hydrothermal carbonization, it also promotes the degradation of lignocellulosic components and also the formation of hydrochar with more total pore volumes

and large specific surface area (Cárdenas-Aguiar, et al., 2019). Hemicellulose structures normally are fully degraded and do not remain in hydrochar products (Reza, et al., 2013).

Table 2.4: Properties of Hydrochar and Biochar from Manure Waste at Different Temperature (Cárdenas-Aguiar, et al., 2019).

<b>Process</b>	<b>Temperature (°C)</b>	<b>Surface area (m<sup>2</sup>/g)</b>	<b>pH</b>	<b>CEC (cmol/kg)</b>
Hydrothermal carbonization	190	14.21	7.3	39.2
	240	14.96	7.8	18.9
Pyrolysis	450	4.82	10.2	63.0
	600	4.67	10.3	50.6

In short, feedstock with high moisture content is more preferable in using the process of hydrothermal carbonization (Xiang, et al., 2020). Several advantages of using hydrothermal carbonization for the preparation of biochar such as the produced biochar has more oxygen functional groups and energy intensive method of drying is not required (Nidheesh, et al., 2020). However, the carbon content in hydrothermal carbonization is not as stable as the pyrolysis process. Prolonged residence time is also needed in this process.

#### **2.4 Modification of Biochar**

Biochar is an adsorbent that can remove contaminants from water. However, it has limited ability in terms of pore structure, functional groups, and surface area which leads to lower efficiency in adsorbing contaminants of high concentrations (Zheng, et al., 2020). Several researchers have shown that the modification of biochar can increase the efficiency of the adsorption of organic and inorganic pollutants in water. Modified biochar is obtained to enhance the functional groups, pore structure and surface area (Ahmed, et al., 2016). Therefore, methods such as magnetic modifications can be done in removing the contaminants of dyes in wastewater treatment.

### 2.4.1 Nano-zerovalent Iron Modified Biochar

In recent years, modification of metal nanoparticles has been extensively applied and brought much attention especially nano-zerovalent iron (nZVI). nZVI serves as a reducing agent and is characterised by large surface adsorption sites, large surface area, high reductive reactivity and possess magnetic property (Eltaweil, et al., 2020). This magnetically modified biochar is environmentally friendly and can be used to remove organic pollutants effectively.

The crystallite size of nZVI is smaller than micron or millimeter-sized particles. When comparing nZVI with zero-valent iron (ZVI), nZVI has a higher reactivity and can degrade organic contaminants more effectively because nZVI has a larger specific surface area (Quan, et al., 2014). As reported by Eltaweil, et al., (2020), nZVI/biochar composite was able to degrade 99.99 % of malachite green dye after 20 minutes. Removal mechanisms such as adsorption, Fenton-like degradation, precipitation, oxidation, reduction, surface complexation and dichlorination can be performed by nZVI. Although nZVI could remove organic contaminants effectively, the small particle size of nZVI would cause agglomeration and precipitation to occur easily due to their large surface area and high surface energy (Zhu, et al., 2017). This showed a clear evidence that nZVI was unstable and modification had been developed to enhance the stability of nZVI. Modification techniques such as using biopolymers, zeolite, carbon materials or activated carbon as a supporting material for immobilization of nZVI (Qian, et al., 2019). When nZVI particles were supporting by solid materials or entrapped in polymers, the stability of nZVI was enhanced and the physicochemical properties also could be improved (Quan, et al., 2014).

Among those supporting materials, biochar is one of the most commonly used supporting materials for nZVI. This is because biochar has a large surface area, porous structure, and a high adsorption capacity towards the pollutants. Biochar is an organic porous material with numerous surface functional groups and prevent aggregation and oxidation (Zhu, et al., 2017). By using biochar to support nZVI also improved the distribution of nZVI particles where the carbon skeleton barrier segregated inside the pores (Wang, et al., 2019a). There are several mechanisms such as coordination, adsorption

being involved during nanoparticle assembling with biochar. Figure 2.2 depicts the oxide shell that surrounds the nZVI core and can react with the surface functional groups of biochar in forming stable bonds. With these, the strength of the intraparticle attraction and aggregation for nZVI can be reduced and subsequently improved the dispersion of nZVI particles.

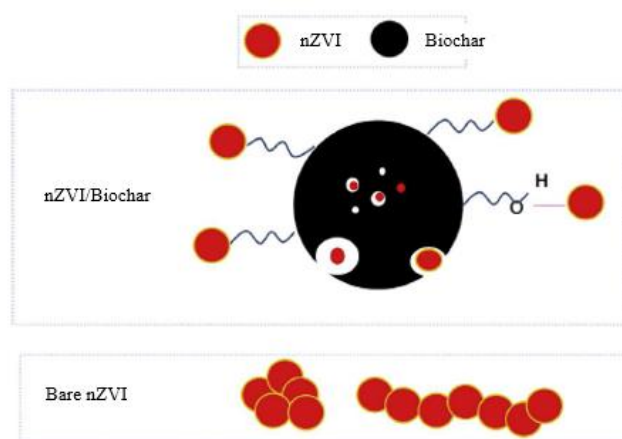


Figure 2.2: Schematic Diagram of Interaction Between Functional Group on Biochar and nZVI (Wang, et al., 2019a).

When using biochar to support nZVI, it could reduce the oxidation tendency (Wang, et al., 2019a). This was due to the porous structure of biochar limited the diffusion oxygen to nZVI and subsequently reducing the exposure to oxidant. Biochar also has certain functional groups such as phenol groups that are resistant to oxidation. Besides, biochar decreases the surface corrosion and leaching of Fe ions from nZVI (Lei, et al., 2018). Fe ions that are inactivated with biochar's functional groups can control the surface corrosion of nZVI.

Electron transfer is also significant for the catalytic process in removing contaminants. Biochar helps to enhance the electron transfer capability of nZVI by accepting or donating electrons with their unique characteristics (Wang, et al., 2019a). Improvement in electron transfer ability of biochar has been ascribed to the surface functional groups and graphene structure (Oh, et al., 2016). When the temperature increasing, the transfer of electrons is easier with increasing graphitization.

## 2.4.2 Carbonaceous Materials

Another modification method of biochar is using carbonaceous material as it helps to increase the surface area of biochar. Carbonaceous materials are organic matters that have functional groups to create strong bonds among the surface of biochar with pollutants in water. For instance, carbon nanotubes and graphene can adsorb organic pollutants such as dyes more effectively and improve the adsorption capacities of biochar (Wang and Wang, 2019). Currently, carbon nanotubes and graphene are widely used in environmental remediation although the preparation costs are high.

Figure 2.3 illustrates that carbon nanotubes consist of cylindrical graphitic sheets where carbon atoms are organized well and located at the edges of hexagons (Sarkar, et al., 2018). Rolling a single graphene sheet provides the result of single-walled carbon nanotubes. Besides, a multi graphene sheet resulting in multi-walled carbon nanotubes after rolled up. There are few properties such as large specific surface area, high chemical stabilities, high thermal stabilities that make carbon nanotubes an attractive material that adsorbs pollutants effectively. Biochar acts as a microporous carrier of carbon nanotubes to form adsorbents for water remediation effectively (Rajapaksha, et al., 2016). The large surface area with the porous structure of biochar can assist in stabilizing the carbon nanotubes.

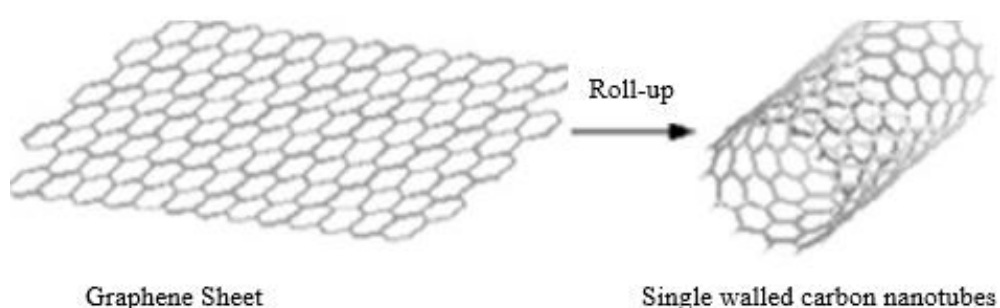


Figure 2.3: Graphene Sheet in Forming Single-walled Carbon Nanotubes (Sarkar, et al., 2018).

Graphene is another carbonaceous material whose graphene oxide is the precursor and able to adsorb heavy metals with great adsorption capacity (Wang and Wang, 2019). Heavy metals can chemically bind with functional

groups that contain oxygen which exists on the surface of graphene oxide. Before pyrolysis, impregnated feedstock in a graphene oxide forms graphene oxide biochar composites and has improved the biochar adsorption capacity (Sizmur, et al., 2017). Besides, this modification of biochar leads to a larger surface area and provides abundant amounts of oxygen-containing functional groups.

### 2.4.3 Metal Oxides

Modification of biochar using metal oxides affects the adsorption sites, magnetism and catalysis. Metal oxides improve the adsorption sites for biochar in pollutants removal (Sizmur, et al., 2017). Biochar possesses the characteristics of low adsorption capacity towards anionic dyes because most of the biochar's surface is negatively charged (Wang and Wang, 2019). However, modification of biochar with metal oxide enhanced the surface properties of biochar and adsorption sites towards anionic dyes. The surface electrochemical properties of biochar also changed from the negatively-charged surface to positively charged in the presence of metal oxides (Xiao, et al., 2018).

To modify biochar, the metal oxide was firstly mixed with feedstock followed by pyrolysis in synthesizing biochar. Another method is to pyrolyse the feedstock when preparing biochar followed by soaking the biochar with metal oxides in certain conditions (Wang and Wang, 2019). Then, there are a few metal oxides based photocatalysts such as titanium dioxide ( $\text{TiO}_2$ ), iron oxide ( $\text{Fe}_3\text{O}_4$ ), zinc oxide ( $\text{ZnO}$ ), and magnesium oxide ( $\text{MgO}$ ) had proved their efficiency in the water treatment process through the degradation of dyes. For instance,  $\text{Fe}_3\text{O}_4$  nanoparticle-loaded biochar derived from the pomelo peel achieved 24.79 mg/g adsorption capacity with the impregnation ratio of 5:1  $\text{Fe}_3\text{O}_4$ /biochar for reactive red 21 dye from an aqueous solution (Nguyen, et al., 2020).

One of the metal oxide nanoparticles commonly used is  $\text{TiO}_2$ .  $\text{TiO}_2$  is commonly used because of its large availability, eco-friendliness, low cost, corrosion resistance and high photo-activity (Pang, et al., 2016). Nevertheless, the bandgap energy of  $\text{TiO}_2$  is wide (3.2 eV) which limits the photocatalytic application. This is because it restricts its ability in absorbing visible light and

only ultraviolet irradiation can be utilized for the excitation process (Cui, et al., 2020). Then, an extra ultraviolet source needs to be accounted for this photocatalytic system since ultraviolet light only accounts for 7 % of the sunlight which is insufficient to excite  $\text{TiO}_2$  photocatalyst. Thus, various methods had been explored to lower down the bandgap energy of  $\text{TiO}_2$  and improved the photocatalytic activity of  $\text{TiO}_2$ . Doping of photocatalysts with additional metallic or non-metallic substances contributes to lower down the bandgap energy of  $\text{TiO}_2$ . Not only that, incorporating  $\text{TiO}_2$  onto a biochar surface also enhanced the performance and at the same time changed the structure, morphology and light absorption efficiency of the composites (Cui, et al., 2020). Although  $\text{TiO}_2$  has wide bandgap energy, biochar modified  $\text{TiO}_2$  composites are used extensively due to their electrostatic interaction, physical adsorption, and suppression of electron charges recombination granted by biochar. These properties encourage its application in the removal of water contaminants during the water treatment process. As reported by Wang, et al., (2018),  $\text{TiO}_2$ /biochar composite derived from bamboo able to achieve a maximum of 97 % methylene blue degradation rates.

Then,  $\text{Fe}_3\text{O}_4$  is another metal oxide that has better efficiency in degrading pollutants. Iron oxide normally exists in numerous forms such as magnetite ( $\text{Fe}_3\text{O}_4$ ), maghemite ( $\gamma\text{-Fe}_2\text{O}_3$ ) and hematite ( $\alpha\text{-Fe}_2\text{O}_3$ ). Figure 2.4 shows the crystal structure for three different types of iron oxides. In  $\alpha\text{-Fe}_2\text{O}_3$ , oxygen atoms are arranged in hexagonal close-packed ferric ( $\text{Fe}^{3+}$ ) ions occupied two of every three octahedral sites and do not have any periodic vacancies (Pang, et al., 2016). Besides, it was observed that the oxygen atoms in  $\text{Fe}_3\text{O}_4$  are arranged in a cubic close-packed with an inverse spinel structure. Then,  $\alpha\text{-Fe}_2\text{O}_3$  has the same crystal structure as  $\text{Fe}_3\text{O}_4$  but there is a slight difference which  $\alpha\text{-Fe}_2\text{O}_3$  has vacant in their sub-lattices and has  $\text{Fe}^{3+}$  (Pang, et al., 2016).

Since there are a few types of iron oxide, they own different magnetic behaviors such as their valence states of iron in sub-lattices.  $\text{Fe}_3\text{O}_4$  has the highest saturation magnetization among these iron oxides considering the adjacent site between both ferrous ( $\text{Fe}^{2+}$ ) ions and  $\text{Fe}^{3+}$  ions which electron delocalization could occur (Pang, et al., 2016). Then,  $\text{Fe}_3\text{O}_4$  is unstable in

oxidizing condition and will be transformed to  $\gamma$ - $\text{Fe}_2\text{O}_3$  and  $\alpha$ - $\text{Fe}_2\text{O}_3$  at high temperature but able to form back to its original through hydrogen reduction of  $\alpha$ - $\text{Fe}_2\text{O}_3$  (Lu, Salabas and Schüth, 2007). Generally, among three different iron oxides, the most common impregnation metal onto a biochar surface is  $\text{Fe}_3\text{O}_4$ . (Wang, et al., 2019). Some researchers have proved that the adsorption efficiency for magnetic biochar by chemical coprecipitation of iron oxides onto biomass before pyrolysis provides better results than other materials (Tan, et al., 2016).

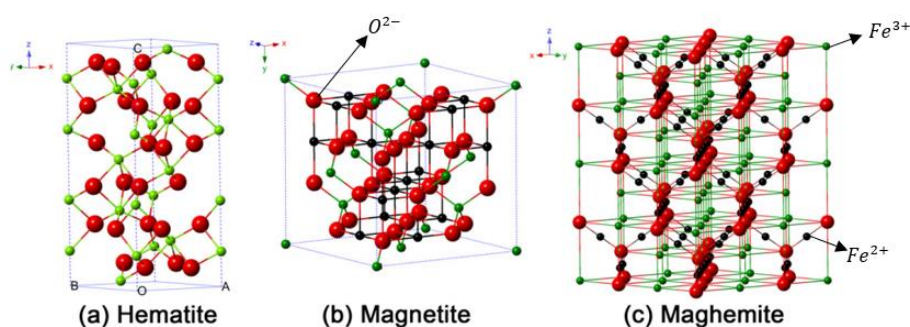


Figure 2.4: Crystal Structure of Different Metal Oxides (Wu, et al., 2015).

In addition, nanoparticles of ZnO are another type of semiconductor photocatalysts (Ubani and Ibrahim, 2019). ZnO is characterised by high stability, high electron availability and strong oxidation ability. However, ZnO has a relatively wide bandgap energy of 3.2 eV, which limiting the photocatalytic application and can only be excited by photons that are close to the ultraviolet region (Pang, et al., 2016). A higher light energy frequency than bandgap energy is absorbed by ZnO. This leading to the creation of a positively charged hole in the valence band (Ubani and Ibrahim, 2019). Not only that, ZnO also has fast recombination for electron-hole pairs due to its wide bandgap energy.

Meanwhile, MgO nanoparticles are the cheapest metal oxide and chemically stable compared to other metal oxides. MgO has a larger surface area and several surface active sites which exhibits high adsorption performance and rapid adsorption rate (Zhu, et al., 2020). MgO which has properties such as high surface to volume ratio, high charge carrier diffusion length, and better adsorption capability promotes its application in the removal

of water pollutants especially anionic compounds (Li, et al., 2015). Zhu, et al. (2020) also demonstrated that the adsorption efficiency towards congo red dye showed a maximum adsorption capacity and also high adsorption ability towards heavy metals. MgO nanoparticles possessed high surface energy, which promotes the tendency for agglomeration. This drawback can be overcome by incorporating MgO onto biochar's surface (Zhu, et al., 2020).

## 2.5 Advanced Oxidation Process

Advanced oxidation processes (AOPs) are one of the most useful ways to degrade organic pollutants in wastewater treatment (Sonawane, Patil and Sonawane, 2018). The process involves the in-situ generation of highly reactive oxidants such as hydroxyl radicals ( $\bullet\text{OH}$ ) to react with pollutants for degradation. Table 2.5 shows the oxidation potential of common oxidants. Table 2.5 illustrates that  $\bullet\text{OH}$  is the most powerful and highly effective oxidant with an oxidation potential of around 2.80 eV.  $\bullet\text{OH}$  also has the ability in reacting with most of the organic contaminants (Rosal and Agüera, 2008). Although fluoride has the highest oxidation potential, it is not widely used because fluoride is not environmentally friendly. The oxidation reaction of radicals and pollutants is the mechanism behind the degradation of the pollutant itself.

Table 2.5: Oxidation Potential of Common Oxidants (Rosal and Agüera, 2008).

Oxidant	Potential $E^\bullet$ , (V, 25 °C)
Fluoride	3.06
Hydroxyl radical	2.80
Atomic oxygen	2.42
Ozone	2.07
Hydrogen peroxide	1.78
Permanganate	1.68
Chlorine dioxide	1.57
Hypochlorous acid	1.49
Chlorine	1.36
Oxygen	1.23

AOPs can also be categorised based on their radicals generation method. The common AOPs used for the degradation of wastewater contaminants are Fenton-based reactions, photolysis, sonolysis, ozone-based processes and heterogeneous photocatalysis (Gautam and Chattopadhyaya, 2016). Using  $\bullet\text{OH}$  as an oxidant, AOPs can eventually convert the organic contaminants into carbon dioxide, water and salts by attacking the target molecules (Sonawane, Patil and Sonawane, 2018). This brought into the degradation of pollutants in water. The organic pollutants are firstly attacked by hydroxyl radicals through radical addition, hydrogen abstraction, radical combination and electron transfer. Then, the reactions promote the generation of carbon-centred radicals. After that, these radicals further react with oxidants such as hydrogen peroxide ( $\text{H}_2\text{O}_2$ ) to produce carbon dioxide, water and inorganic salts (Deng and Zhao, 2015).

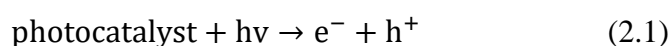
For sulfate radical ( $\text{SO}_4^{\bullet-}$ ) based AOPs, it involves the generation of  $\text{SO}_4^{\bullet-}$  and brought much attention to researchers because it has high redox potential.  $\text{SO}_4^{\bullet-}$  is a highly reactive species with an oxidation potential around 2.6 V (Deng and Zhao, 2015). A few common chemicals can be used to activate sulfate radicals such as peroxymonosulfate (PMS) and peroxydisulfate (PDS). When oxidants are not generating radical species, oxidants are not so reactive. The activation of PMS and PDS is to break hydroperoxide bonds by homolytic or heterolytic cleavage (Duan, et al., 2020). Besides,  $\text{SO}_4^{\bullet-}$  has the tendency to remove electrons from organic molecules followed by transforming organic radical cations (Deng and Zhao, 2015). It reacts with organic compounds through electron transfer by degrading those organic pollutants that contain aromatic and unsaturated bonds efficiently.

### **2.5.1 Photocatalysis**

Photocatalysis is a promising type of advanced oxidation process to treat and degrade organic contaminants in wastewater. Photocatalysis is also an environmentally friendly method in removing hazardous contaminants as it can mineralize organic contaminants completely to form harmless products (Zhu and Zhou, 2019). The photocatalysis process involves the reaction of organic contaminants and powerful reducing and oxidizing agents which are holes ( $\text{h}^+$ ) and electrons ( $\text{e}^-$ ). The generation of  $\text{h}^+$  and  $\text{e}^-$  are from ultraviolet or

visible light on the surfaces of the photocatalyst. However, major drawbacks of this approach include migration ability is low, photo-generated electrons and holes, low-usage of visible light, and fast recombination of charge carriers (Koe, et al., 2019).

In the photocatalysis process, semiconductor photocatalysts such as  $\text{TiO}_2$ ,  $\text{ZnO}$ ,  $\text{Fe}_2\text{O}_3$  are used. The overall mechanism for the photocatalysis process starts from the absorption of light by photocatalysts. The excitation of electrons occurs when the irradiation of the light with the energy equal to or more than the bandgap of the semiconductor photocatalysts (Zhang, et al., 2018c). Electrons are excited from the valence band of the photocatalysts and promoted to the conduction band. Therefore, it leaves the holes behind in the valence band and leads to the formation of electron hole-pairs. Equation (2.1) shows the formation of electron hole-pairs (Zhu and Zhou, 2019).



Then, the generation of electrons and holes might combine easily by the release of heat. Recombination of charge carriers can lead to the low quantum efficiency of the photocatalysts (Zhang, et al., 2018c). Figure 2.5 illustrates the mechanism for photocatalytic activity on a semiconductor's surface. When there is sufficient time for the charge carriers before the recombination process, these electrons and holes will migrate to the surface of the photocatalyst and can undergo charge transfer so that redox reactions can occur with the organic contaminants that are adsorbed on its surface.

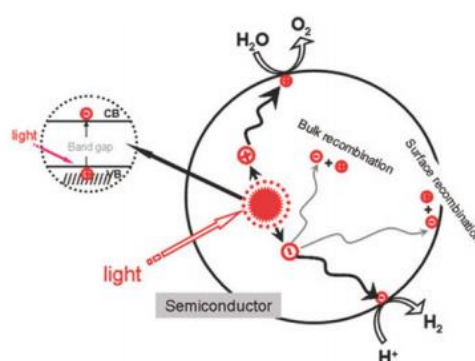
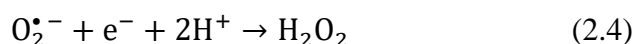
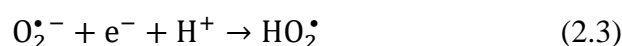
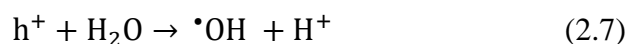


Figure 2.5: Mechanism for Photocatalytic Activity on the Semiconductor Surface (Zhang, et al., 2018c).

In the reduction reaction for photocatalysis, the mechanisms are shown from Equations (2.2) to (2.6) (Zhang, et al., 2018c). During the migration, electrons reached the surface of photocatalysts and reacted with adherent oxygen, strong oxidizing radicals such as hydroperoxyl radical ( $\text{HO}_2^\bullet$ ) and superoxide anion ( $\text{O}_2^{\bullet-}$ ) are produced for the degradation of contaminants in wastewater. The  $\text{O}_2^{\bullet-}$  is then reacts with the electrons and hydrogen ions ( $\text{H}^+$ ) to produce  $\text{HO}_2^\bullet$  and  $\text{H}_2\text{O}_2$ , respectively. The  $\text{H}_2\text{O}_2$  then reacts with the electrons to be further reduced to  $^\bullet\text{OH}$ .



Besides, for the oxidation reaction in photocatalysis, the valence band hole ( $\text{h}^+$ ) has a strong oxidation power and plays a significant role in the photocatalytic degradation of dyes that present on the surface of the catalyst. Equations (2.7) and (2.8) demonstrate the oxidation process taking place through the reaction with  $^\bullet\text{OH}$  or  $\text{h}^+$  attached on metal surfaces (Zhang, et al., 2018c).



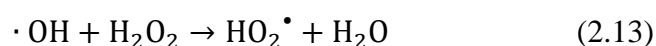
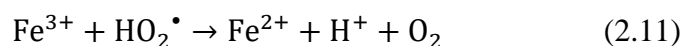
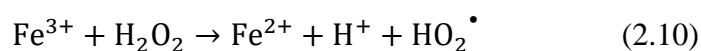
### 2.5.2 Fenton and Fenton-like Processes

In AOPs, the Fenton process is the most frequently used to degrade organic contaminants. The Fenton process is the process that involves the reaction by using  $\text{Fe}^{2+}$  as catalyst and  $\text{H}_2\text{O}_2$  as an oxidant (Wang, et al., 2016). It is widely used nowadays due to its high performance in oxidizing organic pollutants. Besides, the Fenton process is an environmentally friendly approach, which able to convert contaminants into water and oxygen (Hashemian, 2013). The drawbacks of the Fenton process are high operating cost, limited optimum pH

range and a large volume of iron sludge are produced. Therefore, enhancement such as replacing heterogeneous or homogeneous catalysts is applied.

A Fenton-like process can be classified as a homogeneous and heterogeneous Fenton-like process. There are several parameters such as pH, hydrogen peroxide dosage, catalyst dosage and reaction temperature that might affect the Fenton-like process (Wang, et al., 2016). For a homogenous Fenton-like reaction, the catalytic reaction happens in a single phase which is usually in the liquid phase whereas the catalytic reaction in heterogeneous Fenton-like reaction occurs only on the surface of the catalyst. Homogeneous Fenton-like only involves chemical change and no mass transfer limitation. Ferrous ions are usually used as Fenton reagents in homogenous conditions to produce hydroxyl radicals and perhydroxyl radicals ( $O_2H\bullet$ ) (Fontecha-Cámara, et al., 2011). The homogeneous Fenton process also plays an important role to enhance water quality in wastewater treatment. For instance, it decreases toxicity, biological oxygen demand, chemical oxygen demand, and improves biodegradability. Besides, iron catalysts are used as immobilised on a support such as biochar in heterogeneous conditions.

Equation (2.9) shows that the reagent for Fenton is the mixture of  $Fe^{2+}$  ions and  $H_2O_2$  to produce hydroxyl radicals. Then, the reaction of  $Fe^{3+}$  ions as a catalyst in decomposing  $H_2O_2$  to produce hydroperoxyl radical is shown from the Equations (2.11) to (2.15). The removal efficiency of degrading contaminants in the Fenton process can be done by the generation of  $HO_2\bullet$  and  $\bullet OH$ .



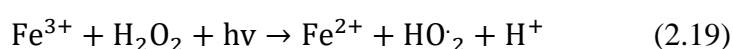
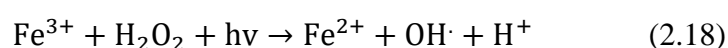
pH is one of the important parameters in the Fenton-like process for effective wastewater treatment. It is highlighted that the optimal pH in a homogenous Fenton reaction for degrading organic pollutants is pH 2.5-3 which is in acidic condition (Wang, et al., 2016). Studies also revealed that when the pH is lower than 2.5, the scavenging effect of hydroxyl radicals occurs leading to stronger  $H^+$  (Wang, et al., 2016). Equation (2.16) shows the scavenging effect of hydroxyl radicals (Fontecha-Cámara, et al., 2011). Besides, different solubilities of metal ions on the catalyst's surface also show different optimal pH in a homogeneous reaction. Certain types of catalysts perform catalytic roles through the dissolution of metal ions from the catalyst surface whereas some catalysts carry out their role through active sites on their surface.



In homogenous conditions, the efficiency in degrading organic contaminants also decreases when there is insufficient  $H_2O_2$  dosage (Jiang, et al., 2010). This also subsequently leads to less amount of  $\bullet OH$  is produced when the pH is at a low condition. Conversely, excessive amount of  $H_2O_2$  dosage would lead to undesirable effect on the reactivity of microorganisms and higher chemical oxygen demand effluent towards treating the wastewater. Not only that, the cost for  $H_2O_2$  dosage also increases when a large amount of wastewater is required to treat (Wang, et al., 2016). Furthermore, optimum catalyst dosage is also significant for both homogeneous and heterogeneous Fenton-like processes. Excessive catalyst dosage would cause  $\bullet OH$  that produced will be consumed by those excess catalysts and also the occurrence of scavenging effect as shown in Equation (2.17). Subsequent effects such as the production cost of solid catalyst also might be the limiting factor for wastewater treatment in heterogeneous Fenton-like processes whereas in homogeneous Fenton-like processes large amounts of sludge are produced leading to the sludge treatment process (Wang, et al., 2016).



In Fenton and Fenton-like processes, catalytic capacity and production of  $\bullet\text{OH}$  improved with the presence of irradiation of ultraviolet light or visible light (Wang, et al., 2016). In the photo-Fenton process, most of the time it is at an optimal pH of 3 and able to enhance the degradation efficiencies for organic pollutants. The generation of  $\text{Fe}^{3+}$  ions behave as light-absorbing species to produce another additional  $\bullet\text{OH}$  as shown in Equation (2.18) and Equation (2.19) (Mirzaei, et al., 2017). The photo-Fenton process requires a lower amount of ferrous catalyst and also produces a lower amount of iron sludge after the reaction. Some researchers have developed the disinfection of treated water due to the inactivation of microorganisms under the irradiation of ultraviolet light (Mirzaei, et al., 2017).



## 2.6 Parameter Study

Parameter studies are significant to determine the efficiency in degrading organic dyes in the water treatment process. There are a few parameters studied such as  $\text{H}_2\text{O}_2$  dosage, catalyst dosage, pH solution, initial concentration of dyes, and temperature for the removal of organic dyes.

### 2.6.1 Effect of $\text{H}_2\text{O}_2$ concentration

In AOPs, the  $\text{H}_2\text{O}_2$  concentration plays a significant role in the degradation efficiency of organic dyes. Generally, an increase of  $\text{H}_2\text{O}_2$  concentration improves the removal efficiency due to the increase of production of  $\bullet\text{OH}$  (Jiang, et al., 2010). Rubeena, et al., (2018) reported that the removal efficiency of Acid Red 1 increased from 67.7 % to 97.6 % using iron-loaded rice husk biochar (Fe-RHB) when the  $\text{H}_2\text{O}_2$  concentration increased from 2 mM to 24 mM in the heterogeneous Fenton process. Similar studies also conducted by Park, et al., (2018) that the degradation rate improved from 29.3 % to 99.7 % with the increase of  $\text{H}_2\text{O}_2$  concentration in degrading Orange G dye using iron impregnated sugarcane bagasse biochar.

Nevertheless, when the  $\text{H}_2\text{O}_2$  concentration increased above the limiting point, degradation efficiency tend to reduce due to the generated

radicals that would react with those excessive primary oxidants to produce less oxidative radicals (Jiang, et al., 2010). Scavenging effects also occurred which led to a decrement in the degradation rate. Therefore, optimum  $\text{H}_2\text{O}_2$  concentration maximized the degradation efficiency for organic contaminants whereas the excessive concentration of  $\text{H}_2\text{O}_2$  decreased the degradation efficiency for organic contaminants.

### **2.6.2 Effect of Catalyst Dosage**

The degradation of organic dyes depends significantly on the dosage of the catalyst. Typically, the higher dosage of catalyst improved the removal efficiency until it reached a certain limit (Li, et al., 2020). This was because the number of active sites available for the catalyst surface increased for the production of  $\bullet\text{OH}$  led to a higher degradation rate of organic pollutants. The statement could be proved with the experiment conducted by researchers. Rubeena, et al., (2018) stated that the dye removal efficiency for iron-loaded coir pith biochar (Fe-CPB) increased from 48.2 % to 81.7 % when the catalyst dosage increased from 1 g/L to 4 g/L. However, the removal rate decreased when the catalyst dosage was further increased to 5 g/L. This might be due to the scavenging reaction that happened between  $\text{Fe}^{2+}$  and  $\bullet\text{OH}$  in the solution (Rubeena, et al., 2018). Excessive catalyst dosage gave a negative impact on the degradation efficiency such as the scavenging effect that led to a decrement in the removal rate of pollutants (Sreeja and Sosamony, 2016). The production cost of the catalyst dosage was one of the limiting factors as a higher dosage of catalyst caused higher cost for treatment of wastewater due to large amount of sludge that might be produced (Wang, et al., 2016).

### **2.6.3 Effect of pH solution**

The pH of the solution is significant in controlling the degradation rates of organic dyes in water. It is highlighted that the pH of the solution can be adjusted with the use of hydrochloric acid (HCl) and sodium hydroxide (NaOH). In the Fenton and Fenton-like process, the optimum pH solution was mostly happened at pH 3. This could be further explained that at low pH,  $\text{Fe}^{2+}$  had lower activity than  $\text{Fe}(\text{OH})^+$  and more  $\text{Fe}(\text{OH})^+$  was formed in Fenton oxidation (Liu, Qiu and Huang, 2011). On the other hand,  $\text{Fe}^{2+}$  could be easily

converted to  $\text{Fe}^{3+}$  and tend to produce a ferric hydrogen complex at pH above 4. At pH above 4, the decomposition of  $\text{H}_2\text{O}_2$  into oxygen and water might occur because  $\text{H}_2\text{O}_2$  was unstable and led to a lower oxidation efficiency (Liu, Qiu and Huang, 2011). Nevertheless, some researchers reported that the optimum pH range in Fenton-like processes was around pH 6 when employing iron oxide/silicon oxide composite (Wang, et al., 2016). This might be due to the solubilities of metal ions present on the surface of the catalyst and the activities that occur on the active sites of the catalyst surface.

In the catalytic process, there are factors such as changes in surface charges and the charge of dye molecules that affect the pH solution. Pang, Lim, and Lee, (2019) reported that the malachite green degradation rate was only 49.88 % at pH 3 whereas the degradation rate increased to 98.5 % when the pH increased from pH 7 to pH 11. This was due to the titanium dioxide/activated carbon catalyst possesses a higher positive charge at low pH solution that improved the interaction with anionic dye molecules. Enhancement of interaction between anionic dye molecules and catalysts was through the electrostatic force of attraction. Nevertheless, too low pH solution brought competitive impacts towards hydrogen ions and subsequently decreased the decolourisation rates (Pang, Lim and Lee, 2019). Thus, the electrostatic repulsion between cationic malachite green and the positive surface charge of catalysts were promoted. Overall, a higher pH solution contributes higher catalytic degradation rate because of the accumulation and production of HOO radicals in bulk liquid providing oxidation in dye molecules.

#### **2.6.4 Effect of Initial Dye Concentration**

The effect of initial dye concentration is also one of the important factors affecting dye degradation efficiency. In AOPs, the degradation rate increased when the initial dye concentration increased. The reaction between  $\bullet\text{OH}$  and dye molecules on the catalyst's surface also increased when the initial concentration increased led to an increment of decolourisation rate. Conversely, the degradation efficiency decreased when it reached the saturation point. Liu, Qiu and Huang, (2011) reported that more  $\text{H}_2\text{O}_2$  was consumed in Fenton processes due to higher dye concentration. This can be

further illustrated that the degradation efficiency decreased after the optimum concentration.

Similar results were found in the sonocatalytic degradation rate of dye, where it was inversely proportional to the initial concentration of dye. Pang, Lim and Lee, (2019) reported that the degradation efficiency decreased from 99.9 % to 49.5 % with the increment of dye concentration from 100 mg/L to 500 mg/L. This might be due to the active sites of the catalyst being fully occupied with a higher concentration of dye molecules. The screening effect would also occur at a higher concentration between dye molecules and the amount of  $\bullet\text{OH}$  generated on the surface of a catalyst that limited the production of free radicals to destroy the pollutants (Khataee, et al., 2017).

## CHAPTER 3

### METHODOLOGY AND WORK PLAN

#### 3.1 Research Methodology

The research methodology is defined as the path which researchers go through by formulating their objectives and problems, followed by presenting their results according to the data found during the research period (Jilcha Sileyew, 2020). The research methodology in a research paper is to allow readers to evaluate the study critically for the overall reliability and validity. Owing to the interest in the preparation of magnetic biochar as a low-cost adsorbent or catalyst to be used in degrading organic pollutants compared to pristine biochar, several strategies were explored in this research study. In this research, it was essential to study the application of modified magnetic biochar in the degradation of organic dyes with advanced oxidation processes. The role of modified magnetic biochar was evaluated based on the studies.

It is well known that an appropriate approach needs to be done when conducting a research study to manage large amount of information (Chen, et al., 2020a). Systematic reviews were employed in this research study to identify and critically evaluate those relevant research as well as gather and analyse data from the research (Liberati, et al., 2009). The objective of the systematic review was to discover all empirical evidence that answered the research question and met the pre-specified inclusion criteria. Bias also was reduced by using explicit and systematic approaches in analysing papers and all relevant data. This enabled us to provide reliable findings from which decisions and conclusions were made (Snyder, 2019). The detailed methodology used to perform in this research study and work plan were discussed in the following section. Planning, searching, screening and reporting were used to understand in depth this research topic. Systematic analysis of relevant published papers was also documented.

##### 3.1.1 Planning

At the beginning of this review, planning was applied to expand on the depth and applicability of the research topic (Chen, et al., 2020a). With planning, the

success of the research project was completed in the given period of time. In addition, it also set a clear path for the researchers to carry out the research more efficiently. Few research questions were identified and defined. For instance, what was the current status of the research on organic dyes in wastewater? How effective was the usage of modified magnetic biochar in the degradation of organic dyes with advanced oxidation processes? Which kinetic models fitted well in the degradation of organic dyes with advanced oxidation processes? Perhaps understanding and defining research questions able to keep the research study more focused and effective.

### **3.1.2 Searching**

Searching is one of the most significant steps in conducting a research study. It is the process of gathering tons of information and journals as much as possible. Yet, the effective search was one of the research strategies implemented to obtain data on highly likely matches and to ensure that there were not too much overwhelming data or too little data. The searching strategy also aided in defining appropriate search strings and identifying relevant databases for the collection of relevant documentation (Mengist, Soromessa and Legese, 2020).

Firstly, analysing and identifying research keywords were done. Keywords were not only important for search engine optimization, but also for the overall content strategy in producing a good report. In this study, the main keywords used were “Advanced Oxidation Process”, “Magnetic Biochar”, and “Organic Dyes”. Besides, alternative keywords such as “Fenton”, “Photo-Fenton”, “Photocatalysis”, and “Organic Pollutant” were also used for replacement of the keywords to get more relevant journals. Synonyms, plurals, phrases and abbreviations were taken into account to ensure more relevant journal papers were obtained. The boolean technique was also used when searching for journals or articles related to creating a very broad or very narrow search.

During the searching process, a few platforms were used to obtain highly reliable data and resources. Online databases such as Elsevier, Wiley Online Library, and Scopus were used which include journals, textbooks and data analysis. All these online databases were accessible through the UTAR

library and were found reliable which they were highly focused on publishing scientific journals. By using multiple databases, it brought up different results although the same search keywords or phrases were entered.

### **3.1.3 Screening and Reporting**

The next step in the research methodology was screening for inclusion or exclusion of the information. Screening is a process of evaluating the applicability of the journals found and eliminating those journals which are irrelevant and lack information (Snyder, 2019). Titles and abstracts from 532 publications were screened initially and evaluated before making the selection. Literature such as inaccessible publications, non-English language papers, presentations and keynotes were removed whereas the remaining articles were retained for further reading. This was to ensure the completeness and fidelity of this research study. Initial screening also had greatly reduced the number of journals that required the detailed reading phase and further analysis (Mengist, Soromessa and Legese, 2020).

After the first screening, the final selection was done by reading the full-text articles to ensure the journal papers selected were of high significance and met the inclusion criteria. During the final screening process, some articles were eliminated due to the information in the journals not being included in the systematic review and did not meet the inclusion criteria. In this review study, the selected journals were focused on investigating the application of modified magnetic biochar for the removal of organic dyes in wastewater with advanced oxidation processes. In terms of pollutants, pollutants such as heavy metals, phenols, and polyaromatic hydrocarbons were excluded. Duplicated journals or articles that contained insufficient results were also removed. The remaining journals were then documented and categorised properly as presented in the structure of the review. Overall, the selected journals were analysed critically and summarised in terms of important features, content and abstract (Chen, et al., 2020a).

## **3.2 Data Collection**

Data is defined as the body of information that can be extracted from different sources such as numbers, hyperlinks, video, words, and audio (Onwuegbuzie

and Frels, 2016). Perhaps, the literature review process was actualised through data collection. The information which was collected and gathered comprehensively for literature review represented the process of data collection. Before collecting the data, outlines for the review study such as the production of biochar, modification of biochar, parameters affecting the degradation of organic dyes and others were listed out and planned to ease the process of data collection in obtaining them. In the collection of data for systematic reviews, the accuracy, completeness and accessibility for future updates of the review were significant.

There are two categories in the methodology for the collection of data which are primary methods of data collection and secondary methods of data collection. Primary data collections also can be said as the original data sources that involve the process of interviews, conducting experiments, surveys, and field observation to collect the data directly which is quite time-consuming (Hox and Boeije, 2004). New data and information are added to the current store of social knowledge whenever primary data are collected. Meanwhile, secondary data collections are by using the data collected previously by other researchers (Hox and Boeije, 2004). For instance, secondary data collections can be obtained from journals, articles or books. During the research study, secondary data collection was used which data collection was done by evaluating the quality requirements for the current research and retrieving relevant data. It was advantageous because the access to collecting relevant data was faster and the cost was lower compared to the primary data collection.

Based on the research title, the data collected in this research mainly focused on the synthesising of magnetic biochar and the application of magnetic biochar in degrading organic dyes with advanced oxidation processes. It was found that there were many synthesis methods in preparing the magnetic biochar and advanced oxidation process including the Fenton process, photo-Fenton process, photocatalytic process and others. The degradation of organic dyes in different processes and the catalytic effect of catalysts were investigated.

### **3.3 Data Analysis**

Data analysis refers to the process of carefully evaluating the information or data collected using analytical and logical reasoning. It is important to know how the journals will be used in conducting an appropriate analysis (Snyder, 2019). Evaluation of synthesised data, extraction of relevant information and concluding the selected papers were all part of the analysis stage (Mengist, Soromessa and Legese, 2020). Besides, formulated research questions were answered in the analysis phase. The analysis of data also includes qualitative and quantitative interpretation and narration of the findings, recommendations for future research works, and making a conclusion as well as a discussion (Mengist, Soromessa and Legese, 2020). There are a variety of analysis methods available when conducting a review study. However, meta-analysis was used in this research study as it was a quantitative and formal approach for systematically evaluating data from articles or journals that had been published by other researchers and inferring a conclusion about that body of research (Haidich, 2014).

There were several benefits such as the improvement in precision and ability in answering formulated questions when the meta-analysis was applied in this study. The outcome in meta-analysis provided precise information by collecting more information and providing convincing evidence (Haidich, 2014). In this review study, the data was analysed by determining the structure and characteristics of the modified magnetic biochar and the catalytic performance of the catalyst in the degradation of organic dyes. The evaluation for the reused modified magnetic biochar was also done by analysing the data obtained from several journals by different researchers. According to Mengist, Soromessa and Legese, (2020), the analysis in data and reporting depended on personal judgement with relevant justifications provided. This also revealed the understanding level of the researchers.

## CHAPTER 4

### RESULTS AND DISCUSSION

#### 4.1 Synthesis of Magnetic Biochar

Research studies showed that magnetic biochar was the most commonly used materials to remove organic dyes. It acts as a catalyst in AOPs such as the Fenton process, photo-Fenton process, photocatalysis process, and others. Methods such as impregnation pyrolysis, chemical co-precipitation and calcination are a couple of common methods used to prepare magnetic biochar. Each method has its advantages and disadvantages respectively.

Diving into the first method, impregnation-pyrolysis started by impregnating biomass into the magnetic precursor solution such as ferric iron salt. This was then followed by placing them in an anoxic environment with limited oxygen for heat treatment (Feng, et al., 2020). The transformation of the magnetic precursor into magnetic particles then occurred through the reduction of gas generated by pyrolysis with biomass activation. Gasses such as carbon monoxide, hydrogen, carbon dioxide, and PAHs were produced. Table 4.1 shows the summary of different feedstock used in producing magnetic biochar by the impregnation-pyrolysis process.

From Table 4.1, Rubeena, et al., (2018) reported that Fe-RHB and Fe-CPB were prepared through the impregnation-pyrolysis as both rice husk and coir pith were firstly placed in the furnace at 700 °C for 5 hours after the drying process. After that, both biochars were added to iron (III) nitrate nonahydrate ( $\text{Fe}(\text{NO}_3)_3 \cdot 9\text{H}_2\text{O}$ ) solution followed by agitated them in sonicator and oven dried for one day. Then, it was placed in the furnace at 500 °C. Park, et al., (2018) also focused on the production of magnetic biochar by utilizing sugarcane bagasse as the biomass through the impregnation pyrolysis process. The biomass was firstly impregnated in iron (II) sulfate heptahydrate ( $\text{FeSO}_4 \cdot 7\text{H}_2\text{O}$ ) solution through vigorous stirring. Then, it was dried at 60 °C for 24 hours followed by pyrolyzing it in the furnace at 600 °C for 4 hours.

Table 4.1: Summary of Impregnation-Pyrolysis on Production of Magnetic Biochar with Different Feedstock.

Feedstock	Reagent	Magnetic Biochar	Operating Conditions	References
Waste tea leaves	FeSO <sub>4</sub> .7H <sub>2</sub> O and Ti(SO <sub>4</sub> ) <sub>2</sub>	Fe <sub>2</sub> O <sub>3</sub> /TiO <sub>2</sub> biochar	<ul style="list-style-type: none"> <li>- Dried leaves were placed into tube furnace at 500 °C under flow of nitrogen atmosphere for 3 hours.</li> <li>- Biochar was pre-treated with HCl for 6 hours at 30 °C.</li> </ul>	(Chen, et al., 2020b)
Sugarcane biochar	FeSO <sub>4</sub> .7H <sub>2</sub> O	Fe-impregnated sugarcane biochar	<ul style="list-style-type: none"> <li>- Obtained mixture heated at 350 °C for 2 hours in tube furnace to get magnetic biochar.</li> <li>- Biomass was dried at 60 °C for 24 hours followed by pyrolyzing in furnace at 600 °C for 4 hours.</li> </ul>	(Park, et al., 2018)
Agar powder	Ti(OBu) <sub>4</sub> , FeCl <sub>3</sub>	TiO <sub>2</sub> -Fe <sub>3</sub> O <sub>4</sub> biochar	<ul style="list-style-type: none"> <li>- Process was carried out at pH 9.</li> <li>- Dried the floc at 60 °C in oven.</li> <li>- Pyrolysis process for solid residues of floc was at 800 °C for 1 hour under flow of nitrogen atmosphere.</li> </ul>	(Mian and Liu, 2019)

Table 4.1 (Continued)

Sawdust	$\text{FeCl}_3 \cdot 6\text{H}_2\text{O}$	Fe biochar	- Residue was dried at 80 °C for 24 hours. - Pyrolyzed the feedstock at 700 °C for 1 hour in nitrogen flow atmosphere.	(Jiang, et al., 2019)
Rice straw	$\text{FeSO}_4 \cdot 7\text{H}_2\text{O}$ and $\text{Co}(\text{NO}_3)_2 \cdot 6\text{H}_2\text{O}$	$\text{CoFe}_2\text{O}_4$ biochar	- Impregnating rice straw in the mixture and water content was evaporated at 80 °C in oven. - The mixture was heated at 800 °C for 4 hours in furnace.	(Liu, et al., 2019)
Rice husk		Fe-RHB	- Collected rice husk and coir pith were dried at 105 °C for 24 hours and placed in the furnace at 700 °C for 5 hours.	(Rubeena, et al., 2018)
Coir pith	$\text{Fe}(\text{NO}_3)_3 \cdot 9\text{H}_2\text{O}$	Fe-CPB	- The biochar was then impregnated in the solution for 30 minutes and oven dried at 105 °C followed by placing them in the furnace at 500 °C for 4 hours.	

Researchers revealed that the amount of time consumed, temperature, and the ratio of biomass used to impregnate magnetic precursors were the factors impacting the production of magnetic biochar. Wang, et al., (2019b) found that  $\alpha$ -Fe<sub>2</sub>O<sub>3</sub> transformed from  $\alpha$ -Fe<sub>2</sub>O<sub>3</sub> into Fe<sub>3</sub>O<sub>4</sub> when the temperature increased from 300 °C to 450 °C. The magnetism of magnetic biochar also increased with the increase of pyrolysis temperature. Iron oxide also tends to convert to zero-valent iron when the temperature was higher than 600 °C (Feng, et al., 2020).

Another method of synthesising magnetic biochar was by chemical co-precipitation. For instance, co-precipitation was performed by distributing the biochar into the magnetic precursor solution and putting the alkaline solution dropwise. This resulted in producing the magnetic biochar as the magnetic precursor formed magnetic precipitation on the biochar's surface. Normally, the magnetic precursor was used with a molar ratio of 1:2 with respect to Fe<sup>2+</sup> and Fe<sup>3+</sup> (Thines, et al., 2017). Table 4.2 shows the production of magnetic biochar by chemical co-precipitation with various feedstocks. Silverorthophosphate (Ag<sub>3</sub>PO<sub>4</sub>)-Fe<sub>3</sub>O<sub>4</sub> activated biochar composite using bamboo as feedstock was obtained via co-precipitation method as described in Table 4.2. The Fe<sub>3</sub>O<sub>4</sub> was obtained when ferric chloride hexahydrate (FeCl<sub>3</sub>.6H<sub>2</sub>O) and ferrous chloride tetrahydrate (FeCl<sub>2</sub>.4H<sub>2</sub>O) were dissolved with HCl and deionized water followed by mixing with a few drops of NaOH solution (Jun, et al., 2020). The solution was then mixed vigorously.

Zhang, et al., (2007) reported that copper ferrite (CuFe<sub>2</sub>O<sub>4</sub>)/activated carbon magnetic composite was prepared by co-precipitation. Coconut powdered activated carbon was added into copper (II) chloride and ferric chloride by mixing with a few drops of NaOH solution to ensure that solution was in an alkaline state. The solution was then brought to boil to a temperature of 100 °C for 2 hours. The magnetic composite was then washed with distilled water after cooling. Fang, et al., (2015) employed the chemical co-precipitation process in producing Ca-Mg biochar. Corncob was suspended with the ratio of 1:3 in magnesium chloride (MgCl<sub>2</sub>) and with the ratio of 1:3 in calcium chloride (CaCl<sub>2</sub>) for 2 hours and dried at 110 °C. Next, it was further heated at 600 °C for 3 hours with nitrogen gas flow.

Table 4.2: Summary of Chemical Co-Precipitation on Production of Magnetic Biochar with Different Feedstock.

Feedstock	Reagent	Magnetic Biochar	Operating Conditions	References
Bamboo	FeCl <sub>3</sub> .6H <sub>2</sub> O, FeCl <sub>2</sub> .4H <sub>2</sub> O and Na <sub>2</sub> HPO <sub>4</sub> .12H <sub>2</sub> O	Ag <sub>3</sub> PO <sub>4</sub> -Fe <sub>3</sub> O <sub>4</sub> activated biochar composite	- Biomass were carbonized at 500 °C for 1.5 hour. - Dissolved FeCl <sub>3</sub> .6H <sub>2</sub> O and FeCl <sub>2</sub> .4H <sub>2</sub> O with HCl and deionized water followed by mixing with NaOH. - Precipitates was dried at 60 °C in oven.	(Jun, et al., 2020)
Coconut powdered	FeCl <sub>3</sub> and CuCl <sub>2</sub>	CuFe <sub>2</sub> O <sub>4</sub> loaded magnetic biochar	- Process was carried out at pH 10. - Suspension was heated to 98°C to 100°C for 2 hours. - The molar ratio of Cu <sup>2+</sup> :Fe <sup>3+</sup> was 1:2.	(Zhang, et al., 2007)
Corncob	CaCl <sub>2</sub> and MgCl <sub>2</sub>	Ca-Mg biochar	- Corncob was suspended with the ratio of 1:3 in MgCl <sub>2</sub> and with the ratio of 1:3 in CaCl <sub>2</sub> and were further heated at 600 °C for 3 hours with nitrogen gas flow.	(Fang, et al., 2015)
Wheat straw	FeCl <sub>3</sub> .6H <sub>2</sub> O and FeSO <sub>4</sub> .7H <sub>2</sub> O	Fe <sub>3</sub> O <sub>4</sub> loaded wheat straw magnetic biochar	- Mixture dissolved in ammonia solution under nitrogen flow with molar ratio of 1:2 of Fe <sup>2+</sup> :Fe <sup>3+</sup> . - The temperature was raised to 70 °C for 4 hours.	(Tian, et al., 2011)
Sugarcane bagasse	FeCl <sub>3</sub> and FeSO <sub>4</sub>	Magnetic modified sugarcane bagasse	- Mixture dissolved in ammonia solution under ultrasound irradiation at 60 °C with a molar ratio of 2:1 of Fe <sup>2+</sup> :Fe <sup>3+</sup> .	(Yu, et al., 2013)

Furthermore, calcination was also used to produce magnetic biochar. Calcination is a thermal process where biochar is heated in the absence of oxygen to remove water, carbon dioxide, sulphur dioxide, and the other volatile substances leading to thermal decomposition (Thines, et al., 2017). Table 4.3 presents the usage of various raw materials in producing magnetic biochar via calcination. Li, et al., (2020) employed calcination by converting cattail into magnetic biochar with the presence of  $\text{FeSO}_4 \cdot 7\text{H}_2\text{O}$  at an increasing temperature from 500 °C to 900 °C under nitrogen atmosphere. Fe species/biochar fiber composite was obtained. Besides, Ma, et al., (2015) employed raw material of corncob for the production of magnetic modified corncob by the calcination process. Magnetic biochar was produced with the presence of  $\text{FeCl}_3 \cdot 6\text{H}_2\text{O}$  at 180 °C in a sealed Teflon autoclave for 6 hours. The calcination process removed impurities while keeping the “core” structure of the corncob. Hence, iron oxide was successfully loaded onto the surface of biochar (Ma, et al., 2015).

In short, synthesising magnetic biochar from different biomass through numerous methods has attracted the researchers’ attention. This was because the modified magnetic biochar was capable of treating wastewater treatment more effectively compared to pristine biochar. The special characteristics of magnetic biochar such as contained abundant oxygenated functional groups, persistent free radicals, magnetic substance, and graphite structure improved the degradation efficiency. Table 4.4 summarises the advantages and limitations of impregnation-pyrolysis, calcination, and chemical co-precipitation. The magnetic biochar products obtained through impregnation pyrolysis were good in stability and less metal leaching. It can be prepared by a one-step process where biomass undergoes pre-treatment only before impregnation without pyrolysis is required (Thines, et al., 2017). Besides, less amount of waste liquid will be produced. However, tar and gas pollutants were produced during the pyrolysis process. The pyrolysis process also required a high pyrolysis temperature that caused higher energy.

Table 4.3: Summary of Calcination on Production of Magnetic Biochar with Different Feedstock.

<b>Feedstock</b>	<b>Reagent</b>	<b>Magnetic Biochar</b>	<b>Operating Conditions</b>	<b>References</b>
Cattail	FeSO <sub>4</sub> .7H <sub>2</sub> O	Fe species/biochar fiber composite	- Calcined at different temperatures under nitrogen atmosphere.	(Li, et al., 2020a)
Corncob	FeCl <sub>3</sub> .6H <sub>2</sub> O	Fe <sub>3</sub> O <sub>4</sub> loaded corncob magnetic biochar	- Calcined at 180 °C for 6 hours.	(Ma, et al., 2015)
Blue green microalgae	FeSO <sub>4</sub> .6H <sub>2</sub> O	Fe <sub>3</sub> O <sub>4</sub> loaded microalgae magnetic biochar	- Calcined in and electric oven for 6 hours at different temperatures	(Peng, et al., 2014)
Rice hull	Ferric acetylacetonate, Fe(C <sub>5</sub> H <sub>7</sub> O <sub>2</sub> ) <sub>3</sub>	Fe <sub>3</sub> O <sub>4</sub> loaded rice hull magnetic biochar	- Calcined at 100 °C for 1 hour in tube furnace.	(Yan, et al., 2015)

Furthermore, chemical co-precipitation was found to be the simplest the process as it only required mixing and heating processes. Similar to impregnation-pyrolysis, magnetic biochar produced through chemical co-precipitation also possessed good stability and less metal leaching. Nevertheless, no excessive temperature required as compared to the impregnation pyrolysis method (Thines, et al., 2017). However, the con is chemical co-precipitation incurs higher cost due to the usage of alkali reagent in both wastewater and the process itself (Feng, et al., 2020). The calcination process is relatively simple to operate and tends to produce materials with controlled size and high magnetism. However, an inert atmosphere is also compulsory during the calcination process.

Table 4.4: Advantages and Limitations for Each Method (Feng, et al., 2020; Thines, et al., 2017).

<b>Method</b>	<b>Advantages</b>	<b>Limitations</b>
Impregnation-pyrolysis	<ul style="list-style-type: none"> <li>• Can be prepared by one step method.</li> <li>• Simple operation.</li> <li>• Obtained magnetic biochar has good stability and less metal leaching.</li> <li>• Less waste liquid produced when preparation.</li> </ul>	<ul style="list-style-type: none"> <li>• During pyrolysis, tar and gas pollutants are produced.</li> <li>• Required higher pyrolysis temperature leads to high energy consumption.</li> <li>• Improper treatment will cause secondary pollutants.</li> </ul>
Chemical co-precipitation	<ul style="list-style-type: none"> <li>• Obtained magnetic biochar has good stability and less metal leaching.</li> <li>• High productivity.</li> <li>• Simplest operation.</li> <li>• Strong controllability.</li> <li>• No excessive temperature is required.</li> </ul>	<ul style="list-style-type: none"> <li>• High cost as large amount of alkali reagents is required.</li> <li>• Alkali wastewaters need to be treated.</li> </ul>
Calcination	<ul style="list-style-type: none"> <li>• Simple operation.</li> <li>• Has the tendency in producing materials with controlled size and high magnetism.</li> </ul>	<ul style="list-style-type: none"> <li>• Requires inert atmosphere.</li> </ul>

## 4.2 Characterisation of Magnetic Biochar

The modified magnetic biochar in this study were synthesised by various synthesis method and feedstock. Thus, characterisation of magnetic biochar such as Scanning Electron Microscopy with Energy Dispersive X-ray Spectroscopy (SEM-EDX), Brunauer-Emmett-Teller (BET) surface area analysis, X-ray Diffraction (XRD) and Fourier Transform Infrared spectroscopy (FTIR) were discussed to determine the physical and chemical properties of magnetic biochar.

### 4.2.1 Scanning Electron Microscope with Energy Dispersive X-Ray (SEM-EDX)

Scanning electron microscopy coupled with energy dispersive X-ray is one of the commonly used techniques to characterise modified magnetic biochar effectively in revealing the morphology of biochar surface which includes the pores and sizes of biochar (Joshi, Bhattacharyya and Ali, 2008). Energy dispersive X-ray spectroscopy is detecting the elemental composition of substance with the aid of SEM. The porous structures of the biochar can determine whether the biochar is an effective adsorbent in adsorbing the dye's contaminant due to the adsorption sites. Moreover, the nanostructures that incorporate biochar surfaces were observed. When particles on the biochar surface agglomerated, this would lead to lower specific surface area and adsorption capacity. There were several researchers found that modifying pure biochar into magnetic biochar showed better separation from aqueous solution due to larger surface area (Islam, et al., 2020).

SEM has been useful in providing information on pore structures with various shapes and sizes depending on the types of modified magnetic biochar. The SEM images obtained by Chen, et al., (2020b) indicated the formation of channels and holes were interconnected between each other for both biochar and  $\text{Fe}_2\text{O}_3/\text{TiO}_2$  biochar as shown in Figure 4.1 (a) to 4.1 (d) due to the carbonization and KOH activation of biochar. An irregular three-dimensional structure with holes and channels was observed in Figure 4.1 (a) to 4.1 (d). However, there were abundantly  $\text{Fe}_2\text{O}_3/\text{TiO}_2$  nanoparticles observed in Figure 4.1 (d). According to Yaashikaa, et al., (2020), biochar that was produced with activation was more porous and possessed a larger surface area compared to

biochar without activation. In the work conducted by Rubeena, et al., (2018), the void spaces of rice husk biochar were filled in with Fe species after the impregnation of Fe. Similar to the results of  $\text{Fe}_2\text{O}_3/\text{TiO}_2$  biochar, the structure of iron rice husk biochar was porous. The loading of iron species on the biochar helped to enlarge the surface area and showed more adsorption capacity (Islam, et al., 2020). Likewise, the structure of iron coir pith biochar also showed porous structure and the void spaces of coir pith biochar filled in with iron species (Rubeena, et al., 2018). The SEM images obtained with EDX analysis proving that a greater amount of Fe content was loaded over coir pith biochar (14.99 %) compared to  $\text{Fe}_2\text{O}_3/\text{TiO}_2$  biochar (6.6 %) and rice husk biochar (5.06 %) (Rubeena, et al., 2018; Chen, et al., 2020b).

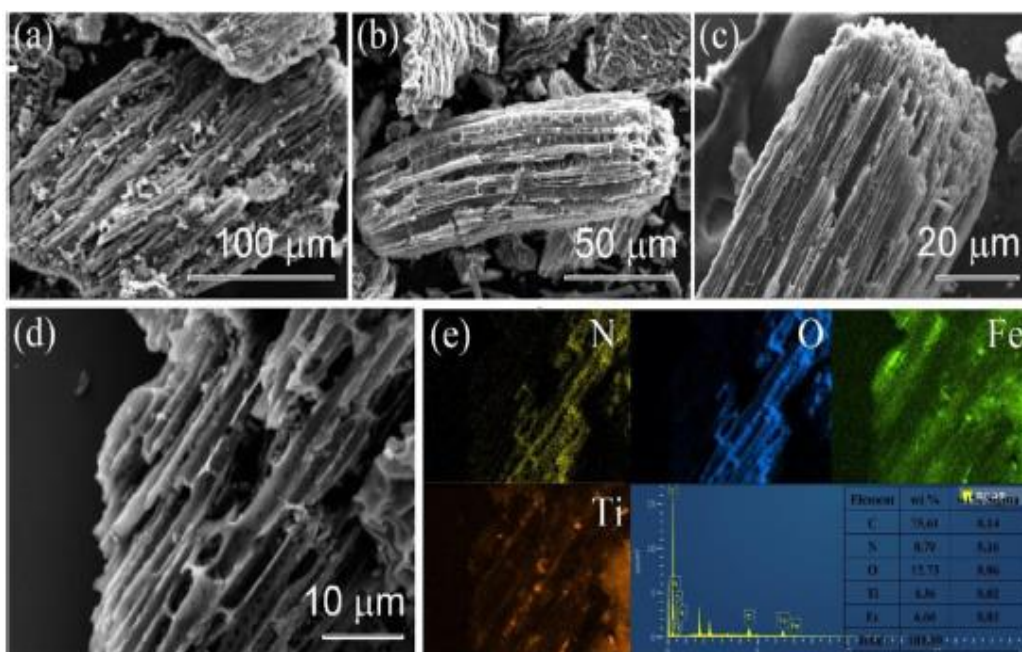


Figure 4.1: SEM Image of (a-c) Biochar (d)  $\text{Fe}_2\text{O}_3/\text{TiO}_2$  Biochar (e) Elemental Mapping (Chen, et al., 2020b).

Furthermore, He, et al., (2020) reported that the shape and structure of iron frass-based biochar (Fe/FBC) were lamellar and tunnel-like with the spherical shape of iron oxide particles distributed on the surface of porous Fe/FBC. Meanwhile, the EDX analysis showed that the Fe content was 6.24 % which was higher than  $\text{Fe}_2\text{O}_3/\text{TiO}_2$  biochar and rice husk biochar mentioned previously. The Fe content loaded on the biochar was different due to the

various mass ratios used when conducting the experiment. According to SEM observations by Li, et al., (2020a), the iron particles were also well distributed on the surface of the biochar. The structure of Fe species/biochar fiber composite was also found porous and had a rough surface. Silva, et al., (2013) also identified similar morphology with He, et al., (2020) showing the spherical shape of iron oxide particles were uniformly distributed with an average diameter of 10 nm on the surface of bamboo biochar. Jun, et al., (2020) reported that the EDX analysis showed that the iron content of bamboo biochar was 47.3 %.

#### **4.2.2 Brunauer-Emmett-Teller (BET) Surface Area Analysis**

BET surface area analysis is to examine the specific surface area and pore distribution of the modified magnetic biochar. It is one of the significant characterisation methods because it contributes to the factor in the degradation of organic dyes. This analysis involves the adsorption of nitrogen on the sample surface. The strong interactions between nitrogen with most of the solids and the availability of high purity made nitrogen the most common choice for gas adsorption (Nasrollahzadeh, et al., 2019). The measurement of the specific surface area can be determined by calculating the amount of adsorption of gas molecules on the sample surface.

Table 4.5 shows the summary of specific surface area for pristine biochar and modified magnetic biochar with its pore volume of various types of magnetic biochar. It was observed that the BET surface area decreased for modified biochar compared to pure biochar. This might be due to the blockages of pore sites or Fe particles filled in some pores thereby decreasing the specific surface area (Li, et al., 2020a). However, Fe/FBC and  $\text{Ag}_3\text{PO}_4\text{-Fe}_3\text{O}_4$  activated biochar composite showed an increase in the specific surface area after modification. The increase in the specific surface area indicated the attachment of the nanoparticles on the surface of the biochar. From Table 4.5,  $\text{CuFe}_2\text{O}_4$  loaded magnetic biochar had the largest specific surface area which was  $555.8 \text{ m}^2/\text{g}$  with  $0.153 \text{ cm}^3/\text{g}$  pore volume. This might be due to the higher amount of lignin in the biomass samples. A larger surface area provided more catalytic active sites for AOPs to take place and facilitate the adsorption of dye molecules. Table 4.5 illustrates the specific surface area and pore volume of

different modified magnetic biochar had different results. The different specific surface areas of different modified magnetic biochar also due to the different thermal degradation and the content of lignin and cellulose (Tomczyk, Sokołowska and Boguta, 2020).

In short, modified magnetic biochar showed better dye degradation efficiency although some of the pure biochar had a larger specific surface area than modified biochar. Park, et al., (2018) reported that the pristine biochar had lower degradation efficiency than iron impregnated sugarcane biochar for Orange G dye proving that the active components loaded on biochar contributed more to the adsorption of dye molecules.

Table 4.5: Specific Surface Area and Pore Volume of Different Magnetic Biochar.

Modified magnetic biochar	Specific surface area (m <sup>2</sup> /g)		Pore volume (cm <sup>3</sup> /g)	References
	Pure biochar	Modified biochar		
Fe <sub>2</sub> O <sub>3</sub> /TiO <sub>2</sub> biochar	-	244.8	-	(Chen, et al., 2020b)
Fe/sugarcane biochar	224.6	179.5	0.1502	(Park, et al., 2018)
Fe/FBC	53.88	90.65	0.1586	(He, et al., 2020)
Fe/biochar fiber composite	746.3	509.8	0.2716	(Li, et al., 2020a)
Ag <sub>3</sub> PO <sub>4</sub> -Fe <sub>3</sub> O <sub>4</sub> activated biochar composite	2.060	4.280	0.0442	(Jun, et al., 2020)
Fe <sub>3</sub> O <sub>4</sub> /corncob magnetic biochar	153.9	69.45	0.1800	(Ma, et al., 2015)
CuFe <sub>2</sub> O <sub>4</sub> /magnetic biochar	799.0	558.0	0.1530	(Zhang, et al., 2007)

#### 4.2.3 X-Ray Diffraction (XRD) Analysis

XRD is a technique that can be used to determine the structure and crystallinity of magnetic biochar (Patel and Parsania, 2017). XRD also has

been useful in proving the successful incorporation of particle phase on biochar. The formation of nanocrystals as the crystalline nature resembles the XRD peaks. Therefore, XRD patterns are able to produce fast, high quality and non-destructive biochar with high sorption efficiency (Yaashikaa, et al., 2020).

Chen, et al., (2020b) reported that the XRD graph of waste tea leaves biochar had a broad and strong diffraction peak centred at  $20^\circ$  to  $28^\circ$  indicating the biochar was in an amorphous phase structure. For  $\text{Fe}_2\text{O}_3/\text{TiO}_2$  biochar, the diffraction peaks at  $24.09^\circ$ ,  $33.16^\circ$ ,  $35.56^\circ$ ,  $40.86^\circ$ ,  $49.47^\circ$ ,  $54.07^\circ$ ,  $62.46^\circ$ , and  $63.98^\circ$  were attributed to  $\text{Fe}_2\text{O}_3$  whereas the peaks at  $23.32^\circ$ ,  $33.07^\circ$ ,  $34.78^\circ$ ,  $40.26^\circ$ ,  $48.73^\circ$ ,  $53.89^\circ$ ,  $62.38^\circ$ , and  $63.67^\circ$  were attributed to  $\text{TiO}_2$  (Singh, et al., 2019). The peaks for  $\text{Fe}_2\text{O}_3/\text{TiO}_2$  biochar were stronger and narrower indicating high crystallinity. It also proved that the  $\text{Fe}_2\text{O}_3/\text{TiO}_2$  nanoparticles loaded successfully on the biochar which ease the separation process during the adsorption of dyes. In the work developed by He, et al., (2020), the diffraction peak of FBC at  $14^\circ$ ,  $24^\circ$ ,  $42^\circ$  corresponded to the reflection from (1 0 1), (0 0 2), and (1 0 0) planes of biochar respectively. After Fe loaded on FBC, no new diffraction peak was observed because Fe/FBC catalyst was stable. Gong, et al., (2013) also claimed that iron oxides loaded on the biochar were low load content and the particle size was small leading to no crystal structure of iron oxides being discovered in Fe/FBC.

Li, et al., (2020a) showed that by increasing the calcination temperature from  $500^\circ\text{C}$  to  $600^\circ\text{C}$ , phase transformation occurred from hematite iron oxide converted to  $\text{Fe}_3\text{O}_4$  in Fe species/biochar fiber composite. The crystallinity of  $\text{Fe}^\circ$  content also increased by increasing the calcining time at  $800^\circ\text{C}$ . Besides, broad diffraction at  $2\theta = 23.05^\circ$  was identified revealing poor crystallization of graphite and amorphous structure (Wang, et al., 2015). Other peaks at  $18.8^\circ$ ,  $20.5^\circ$ , and  $26.8^\circ$  were also identified. The result obtained from Li, et al., (2020a) was similar to He, et al., (2020) as there were no new diffraction peaks detected on Fe species/biochar fiber composite compared with biochar fiber composite due to the low content of self-floating spherical beads. According to Mian, et al., (2019), the peak at  $18.3^\circ$ ,  $30.1^\circ$ ,  $35.4^\circ$ ,  $37.1^\circ$ , and  $56.9^\circ$  was ascribed to the iron phase structure while  $\alpha\text{-Fe}_2\text{O}_3$  attributed to the peak at  $24.1^\circ$ ,  $33.1^\circ$ ,  $40.8^\circ$ ,  $43.5^\circ$ ,  $49.4^\circ$  for N doped (N)- $\text{TiO}_2\text{-Fe}_3\text{O}_4$ -

biochar.  $\text{TiO}_2$  was also found exhibited in the form of anatase and rutile structure. In the work developed by Jun, et al., (2020), the XRD spectrum of  $\text{Ag}_3\text{PO}_4\text{-Fe}_3\text{O}_4$  activated biochar composite presented diffraction peaks at  $33.3^\circ$ ,  $36.6^\circ$ ,  $47.9^\circ$ ,  $52.8^\circ$ ,  $55.1^\circ$  corresponded to the (2 1 0), (2 1 1), (3 1 0), (2 2 2), and (3 2 0) planes of pure  $\text{Ag}_3\text{PO}_4$ . Other diffraction peaks were also determined indicating  $\text{Ag}_3\text{PO}_4$  and  $\text{Fe}_3\text{O}_4$  were successfully loaded on biochar.

#### 4.2.4 Fourier Transform Infrared Spectroscopy (FTIR)

FTIR is another characterisation technique that is used in obtaining an infrared spectrum of absorption and emission of gas, solid, and liquid samples (Sindhu, Binod and Pandey, 2015). It was used to analyse and characterise the functional groups that present on magnetic biochar surfaces. The functional groups available for the magnetic biochar and the interactions between the adsorbent surface with the dye compounds are significant towards the adsorption process.

Chen, et al., (2020b) reported that the bond stretching vibration wavelength for waste tea leaves biochar at  $3455\text{ cm}^{-1}$ ,  $1588\text{ cm}^{-1}$ ,  $1034\text{ cm}^{-1}$ ,  $882\text{ cm}^{-1}$ ,  $815\text{ cm}^{-1}$ ,  $753\text{ cm}^{-1}$ , and  $579\text{ cm}^{-1}$  were assigned to -OH, C=C, C-O, C-H, O=C-O, C-H, and C-H groups. For  $\text{Fe}_2\text{O}_3/\text{TiO}_2$  biochar waste tea leaves biochar, the adsorption peak which centred at  $462\text{ cm}^{-1}$ , and  $431\text{ cm}^{-1}$  were ascribed to the bending vibrations of M-O (Fe/Ti) whereas the peaks at  $700\text{--}900\text{ cm}^{-1}$  in the FTIR spectrum were attributed to the vibrations of Ti-O or Fe-O bond. This indicated that the impregnation of  $\text{Fe}_2\text{O}_3/\text{TiO}_2$  nanoparticles were loaded on the surface of biochar successfully and broadened the peaks which will be more functional to the dye removal. Meanwhile, Park, et al., (2018) claimed that iron impregnated sugarcane biochar and sugarcane biochar were observed in the band range of approximately  $1600\text{ cm}^{-1}$  to  $1595\text{ cm}^{-1}$  corresponding to aromatic C=C and C=O stretching. The high peaks from  $500\text{ cm}^{-1}$  to  $550\text{ cm}^{-1}$  were assigned to the iron particles on the surface of Fe-impregnated sugarcane biochar which helped in degrading dye molecules more efficiently. Similar bond stretching vibration wavelength obtained from He, et al., (2020) for Fe/FBC at around  $3393\text{ cm}^{-1}$  and  $1570\text{ cm}^{-1}$  were found corresponding to the stretching of -OH groups and aromatic ring C=C.

According to Weng, et al., (2013), the peaks of FTIR spectra for both biochar fiber composite and Fe species/biochar fiber composite were observed at  $3415\text{ cm}^{-1}$ ,  $1578\text{ cm}^{-1}$ , and  $1050\text{ cm}^{-1}$ . These bands were attributed to -OH groups, stretching of aromatic C=C groups and C-H bending vibrations, respectively. Peaks at  $458\text{ cm}^{-1}$ , and  $587\text{ cm}^{-1}$  in the FTIR spectrum of Fe species/biochar fiber composite proving that iron-based composite was successfully loaded. This was also associated with the stretching of Fe-O. Mian, et al., (2019) stated that the adsorption peaks for N-TiO<sub>2</sub>-Fe<sub>3</sub>O<sub>4</sub>-biochar at  $476\text{ cm}^{-1}$ ,  $588\text{ cm}^{-1}$ ,  $1149\text{ cm}^{-1}$ ,  $1410\text{ cm}^{-1}$ , and  $1520\text{ cm}^{-1}$  were attributed to the presence of the vibration and stretching for Ti-O, Fe-O, C-O-C of polysaccharides, and OH groups deformation respectively. Likewise, Jun, et al., (2020) reported the stretching of -OH groups was also found in activated biochar at the peak of  $3500\text{ cm}^{-1}$ . A sharp peak was observed at  $968\text{ cm}^{-1}$  for Ag<sub>3</sub>PO<sub>4</sub>-Fe<sub>3</sub>O<sub>4</sub> activated biochar composite, which attributed to the stretching of P-O and vibrations of phosphate ions (Gao, et al., 2017).

### 4.3 Mechanism for Dye Removal

It is well known that the catalytic performance of magnetic biochar catalysts in AOPs are good in treating organic pollutants. Various kinds of AOPs such as Fenton, Fenton-like, photo-Fenton are available, each of them has their respective catalytic mechanism when degrading the dye pollutant.

In the heterogeneous Fenton process, the leaching characteristic was significant in affecting the dye removal mechanism using heterogeneous Fenton catalysts. For instance, Fe-RHB and Fe-CPB possessed low leaching properties with high chemical stability. Figure 4.2 shows the removal mechanism of Acid Red 1 with the iron impregnated biochar catalyst. The activation of H<sub>2</sub>O<sub>2</sub> by Fe<sup>2+</sup> in producing •OH is shown in Equation (4.1) (Feng, et al., 2020). The reactions between iron and H<sub>2</sub>O<sub>2</sub> happened on the surface of the catalyst and it was found that ferric oxide, ferric oxyhydroxide and magnetite were the main oxides that existing on biochar's surface. All other iron minerals contained only Fe<sup>3+</sup> ions except magnetite which contained both Fe<sup>3+</sup> and Fe<sup>2+</sup> ions. Magnetite containing both Fe<sup>3+</sup> and Fe<sup>2+</sup> ions reacted with H<sub>2</sub>O<sub>2</sub> to produce •OH and Fe<sup>2+</sup>, respectively. Then, dye molecules were attacked by •OH within its short lifespan. Equation (4.2) to (4.3) show the

regeneration of ferrous ions in the presence of perhydroxyl radicals and hydrogen peroxide (Feng, et al., 2020). It ensures that the active  $\text{Fe}^{2+}$  always at the heterogeneous catalyst's surface (Rubeena, et al., 2018).

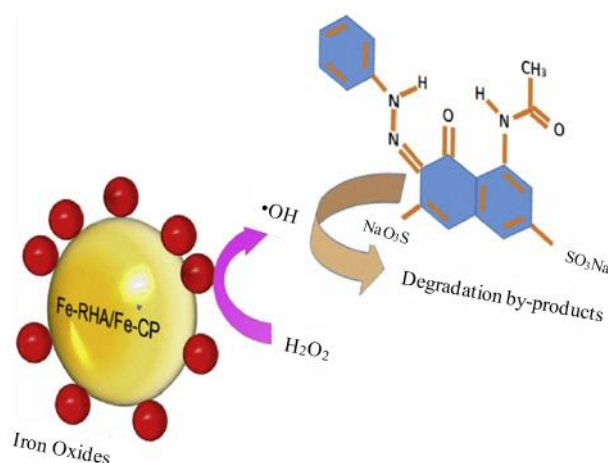
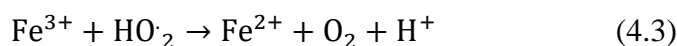
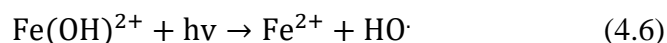
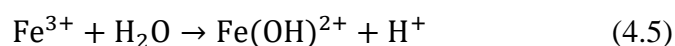


Figure 4.2: Dye Removal Mechanism of Fe-impregnated Biochar Catalyst (Rubeena, et al., 2018).

The biochar matrix in magnetic biochar performed well in electron transfer throughout the Fenton reaction. Biochar matrix in magnetic biochar acts as an electron transfer mediator that helps to enhance the catalytic efficiency. The iron oxides can be further stabilised with the protection and adsorption of the biochar matrix. Parameters such as catalyst dosage, pH, temperature, and hydrogen peroxide dosage affected the catalytic effect in the Fenton process. A similar mechanism was employed for the degradation of methylene blue in the Fenton reaction with  $\text{Fe}_2\text{O}_3/\text{TiO}_2$  biochar as the catalyst.  $\text{H}_2\text{O}_2$  was activated by ferrous ions during the production of  $\cdot\text{OH}$ . Methylene blue was an azo dye in which the pollutants were adsorbed by the abundance of channels and catalyst pores (Chen, et al., 2020b). During the degradation process,  $\cdot\text{O}_2^-$  and  $\cdot\text{OH}$  were produced to attack the dye molecules and form some intermediates products (Chen, et al., 2020b).

Besides, the catalytic efficiency improved with the introduction of light into the Fenton reaction with Fe/FBC. Equation (4.4) shows the decomposition of  $\text{H}_2\text{O}_2$  into  $\bullet\text{OH}$  under ultraviolet-vis light irradiation (He, et al., 2020). Meanwhile, Equations (4.5) to (4.6) illustrate the ability of ultraviolet-vis light irradiation in promoting the reduction of ferric ions and the circulation between both ferrous and ferric ions were accelerated (He, et al., 2020). These also contributed to the removal of malachite green dye with Fe/FBC. Whenever there was an addition of light, the excitation of dye molecules also promoted the generation of photosensitisers molecules which can further produce active species and promote the reduction of ferric ions (Feng, et al., 2020). Generally, the introduction of light into the Fenton reaction enhanced the degradation of malachite green dye for Fe/FBC besides accelerating the Fenton reaction (He, et al., 2020).



Mian, et al., (2019) reported that the mechanism in degrading methylene blue dye with  $\text{TiO}_2\text{-Fe}_3\text{O}_4\text{-biochar}$  in the photo-Fenton process is shown in Figure 4.3. The reduction of  $\text{Fe}^{3+}$  to  $\text{Fe}^{2+}$  occurred when  $\text{Fe}^{3+}$  accepted the electron and reacted with  $\text{H}_2\text{O}_2$  to produce  $\bullet\text{OH}$ . Then,  $\text{Fe}^{2+}$  was further regenerated through the reaction between  $\text{Fe}^{3+}$  and  $\bullet\text{OH}$ .  $\text{O}_2$  reacted with the electron ( $e^-$ ) conductive phase to produce  $\bullet\text{OH}$  and  $\bullet\text{O}_2^-$  to degrade methylene blue dye.

In photocatalysis process, the removal mechanism of magnetic biochar was segmented into four parts. They were the the light absorption by photocatalyst, production of photogenerated electron-hole pairs, the transition of charge carriers and reactant's use of charge carriers (Feng, et al., 2020). For further illustration, bismuth oxybromide ( $\text{BiOBr}$ )- $\text{Fe}_3\text{O}_4$  biochar was used to describe the mechanism of magnetic biochar photocatalysis in degrading organic pollutants. The electron-hole pairs of  $\text{BiOBr}$  and  $\text{Fe}_3\text{O}_4$  were separated under light irradiation (Li, et al., 2019). The valence bands and conduction bands of  $\text{BiOBr}$  and  $\text{Fe}_3\text{O}_4$  were then brought to separation of electron-hole

pair at the interface of the heterojunction structures. Following the separation, the photogenerated  $e^-$  at the conduction band of  $Fe_3O_4$  migrated to the conduction band of  $BiOBr$  whereas holes ( $h^+$ ) at the valence band of  $BiOBr$  transferred to the valence band of  $Fe_3O_4$ . After that, the  $\bullet O_2^-$  was generated through the reaction of  $O_2$  on the surface and  $e^-$  at the conduction band.  $H^+$  on the valence band then reacted with  $H_2O$  to produce  $\bullet OH$  (Li, et al., 2019). Hence, the organic dye was degraded by the active species such as  $\bullet O_2^-$  and  $\bullet OH$ .

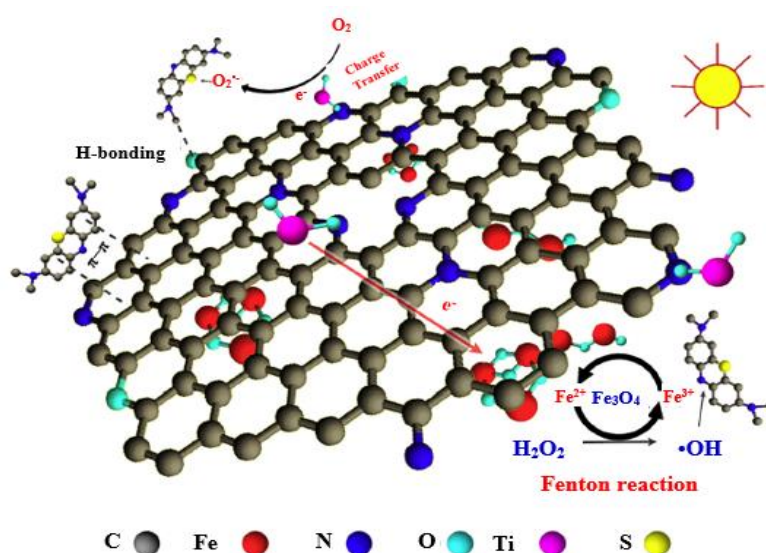


Figure 4.3: Mechanism of Methylene Blue Degradation with  $TiO_2$ - $Fe_3O_4$ -Biochar Catalyst (Mian, et al., 2019).

#### 4.4 Kinetic Study

Kinetic studies are important in the degradation of organic pollutants to understand and reveal the potential reaction mechanisms. Depending on how the activities are accessed, different kinetics affect the degradation process (Riaz, et al., 2020). Pseudo-first order and pseudo-second order kinetic models were the most commonly used kinetic models in dye degradation with AOPs. Generally, the experimental data for dye degradation was fitted to various kinetic equations for quantitative evaluation to determine the suitable model for representation the kinetics of degradation. Table 4.6 shows the kinetic model of dye degradation of modified magnetic biochar in AOPs. It was observed that most of the kinetic data fitted well with pseudo-first order model.

Wang, Huang and Sun, (2020) utilized nZVI/biochar as catalyst in the degradation of methylene blue in the Fenton process. Kinetic model study was conducted by fitting the experimental data acquired using methylene blue at different solution temperature into pseudo-first order kinetic model. They found that the experimental data fitted well with pseudo-first order kinetic model with a correlation coefficient ( $R^2$ ) value which was larger than 0.97. Similar results were also found in the degradation of methylene blue with  $\text{Fe}_2\text{O}_3/\text{TiO}_2$  biochar in the Fenton process. The Fenton reaction was followed pseudo-first order kinetic models and provided the highest degradation efficiency with a rate constant of  $0.101 \text{ min}^{-1}$ . Chen, et al., (2020b) claimed that pseudo-first order was the best fit kinetic model for the degradation of Rhodamine B in Fenton reaction at the rate constant of  $3.7 \times 10^{-2} \text{ min}^{-1}$  with  $\text{Fe}_2\text{O}_3/\text{TiO}_2$  biochar.

Meanwhile, Xu, et al., (2020) reported that the experimental data in degrading methylene blue via Fenton process using iron-derived rubber bark biochar was well fitted well by a pseudo-second order kinetic model. Zang, et al., (2020) found that pseudo-second order was suggested as the suitable kinetic model in the degradation of Rhodamine B with the activation of PMS. Moreover, Li, et al., (2020) reported the  $R^2$  value in pseudo-second order kinetic value for methyl orange degradation was greater than 0.99 with Fe species/biochar fiber composite in photo-Fenton process. The experimental data well fitted pseudo-second order kinetic model and also indicated that there were more electrons involved in the reduction of  $\text{Fe}^{3+}$ . This concluded that both pseudo-first order and pseudo-second order kinetic models were fitted in the experimental data. The kinetic data that followed pseudo-first order kinetic models indicated that the process was mainly physisorption whereas pseudo-second order kinetic models showed that the process was mainly chemisorption (Phan, et al., 2018).

Table 4.6: Kinetic Model of Dye Degradation of Modified Magnetic Biochar with AOPs.

<b>Process</b>	<b>Catalyst</b>	<b>Dye</b>	<b>Kinetic model</b>	<b>References</b>
Fenton	Fe-RHB	Acid red 1	Pseudo-first order	(Rubeena, et al., 2018)
Fenton	Fe-CPB	Acid red 1	Pseudo-first order	(Rubeena, et al., 2018)
Fenton	Fe <sub>2</sub> O <sub>3</sub> /TiO <sub>2</sub> biochar	Methylene blue	Pseudo-first order	(Chen, et al., 2020b)
Fenton-like	nZVI/biochar	Methylene blue	Pseudo-first order	(Wang, Huang and Sun, 2020)
Fenton Oxidation	Fe-biochar	Methylene blue	Pseudo-second order	(Xu, et al., 2020)
Fenton	Fe <sub>2</sub> O <sub>3</sub> /TiO <sub>2</sub> biochar	Rhodamine B	Pseudo-first order	(Chen, et al., 2020b)
Activated PMS	Fe-doped biochar	Rhodamine B	Pseudo-second order	(Zang, et al., 2020)
Fenton	Fe <sub>2</sub> O <sub>3</sub> /TiO <sub>2</sub> biochar	Methyl orange	Pseudo-first order	(Chen, et al., 2020b)
Photo-Fenton	Fe species/biochar fiber composite	Methyl orange	Pseudo-second order	(Li, et al., 2020a)
Fenton	Fe-impregnated sugarcane biochar	Orange G	Pseudo-first order	(Park, et al., 2018)

#### 4.5 Stability and Reusability of Magnetic Biochar

The stability and reusability of magnetic biochar are playing significant roles in the application of modified magnetic biochar. In recent developments, researchers have been studying the effect of these factors on operational cost and its catalytic effect (Gan, et al., 2020). They found that reusing magnetic biochar several times could actually reduce waste effectively. It also possesses excellent magnetic properties, allowing this composite to be removed using magnetic separation. Feng, et al., (2020) revealed that it was notable that the characterisation of magnetic biochar catalyst using electron microscopy, FTIR, X-Ray Photoelectron Spectroscopy (XPS), XRD and Raman spectroscopy did not alter the stability of magnetic biochar. Although magnetic biochar catalysts possessed great stability, the specific surface area decreased due to the adsorption of the organic dyes on magnetic biochar. Table 4.7 shows the catalytic effect of reused modified magnetic biochar catalysts.

He, et al., (2020) reported that even if the magnetic biochar catalyst was reused for 10 cycles in the photo Fenton-like process, the amount of iron leaching for Fe/FBC was only in the range of 0.36-0.76 mg/L. This was less than the legal limit of the European Union which was 2 mg/L. The amount of iron leaching was also attributed to 2.4-5.1 % of the loaded iron content (He, et al., 2020). Hence, the reusability of magnetic biochar did not affect the catalytic property as it was found that the removal efficiency for malachite green dye was still above 98 %. In the degradation of Acid Red 1, the concentration of iron leaching for both Fe-RHB and Fe-CPB were less than 2 mg/L (Rubeena, et al., 2018). This could be further explained that the iron leaching into the solution was insignificant, proving the stability of Fe-RHB and Fe-CPB. After reusing it for 4 cycles, the removal efficiency for Fe-RHB and Fe-CPB were still above 85 % showing that an excellent catalytic effect was maintained despite the reduction of degradation efficiency. The slight decrease in removal efficiency after several cycles of reusing might be due to the leaching and oxidising metals occurring on the surface (Feng, et al., 2020).

Table 4.7: Catalytic Effect of Reused Modified Magnetic Biochar Catalysts.

Process	Catalyst	Dye	Initial Removal Efficiency (%)	Number of Cycles	Removal Efficiency of Last Cycles (%)	References
Fenton	Fe-RHB	Acid red 1	97.60	4	85.30	(Rubeena, et al., 2018)
Fenton	Fe-CPB	Acid red 1	99.10	4	89.40	(Rubeena, et al., 2018)
Fenton	Fe <sub>2</sub> O <sub>3</sub> /TiO <sub>2</sub> biochar	Methylene blue	78.00	5	66.10	(Chen, et al., 2020b)
Fenton	Magnetic biochar derived from sludge	Methylene blue	98.00	5	85.00	(Zhang, et al., 2018b)
Fenton	Fe-biochar	Methylene blue	99.90	4	95.00	(Park, et al., 2020)
Fenton	Fe-impregnated sugarcane biochar	Orange G	99.70	4	89.30	(Park, et al., 2018)
Photo-Fenton like	Fe/FBC	Malachite green	98.30	10	>98.00	(He, et al., 2020)
Photo-Fenton	N-TiO <sub>2</sub> -Fe <sub>3</sub> O <sub>4</sub> -biochar	Methylene blue	99.99	5	89.0	(Mian, et al., 2019)
Sonocatalytic	Ag <sub>3</sub> PO <sub>4</sub> -Fe <sub>3</sub> O <sub>4</sub> activated biochar composite	Rhodamine B	99.00	3	98.01	(Jun, et al., 2020)

According to Chen, et al., (2020b), the reusability and stability of  $\text{Fe}_2\text{O}_3/\text{TiO}_2$  biochar were higher during dye pollutants degradation in the Fenton process. It was found that the methylene blue removal efficiency decreased from 78 % to 66.1 % after undergoing five sets of consecutive runs. Meanwhile,  $\text{N-TiO}_2\text{-Fe}_3\text{O}_4$ -biochar showed better results in degrading methylene blue compared to  $\text{Fe}_2\text{O}_3/\text{TiO}_2$  biochar as the removal efficiency was able to maintain up to 89 % in the fifth cycle (Mian, et al., 2019). This might be due to the different processes used in degrading the dye pollutant involving the presence of sunlight. Besides, various methods of preparing magnetic biochar also influenced its stability. Likewise, magnetic biochar derived from sludge had a removal efficiency of 85 % after conducting five successive methylene blue degradation. Zhang, et al., (2018b) reported that the removal efficiency decreased in the fifth run because of the deactivation of catalyst through the deposition of the small molecule of dye pollutants on its surface.

In another study conducted by Park, et al., (2020), they reported that the degradation rate of methylene blue slightly decreased from 99.9 % to 95 % after four consecutive runs in heterogeneous Fenton reaction. The degradation efficiency decreased after reusing the catalyst multiple times due to the deactivation of catalyst or the difficulty to remove the reaction residues completely and the intermediates bound to the catalyst's active sites. Furthermore, Fe-impregnated sugarcane biochar also possessed high reusability as there was only a slight decrease in the removal efficiency which was from 99.7 % to 89.3 % in the degradation of Orange G after 4 successive Fenton oxidation (Park, et al., 2018). It was also found that there were no massive differences in the removal of Orange G dye proving the Fe-impregnated sugarcane biochar was stable despite the slight drop in removal efficiency following a high number of successive reactions.

In short, magnetic biochar acts as a low-cost catalyst and is easily separable magnetically. It is also reusable while remaining stable after the removal of organic dyes in AOPs. From Table 4.7, it can be deduced that the removal efficiency of magnetic biochar catalysts decreased after multiples recycle. Nevertheless, the resulted degradation rates after a few times of successive reactions were still high. The decreased removal efficiency might

be due to the attached organic matter causing the blockage in active catalytic sites (Gan, et al., 2020). It was also found that no structural and morphological alterations took place.

## CHAPTER 5

### CONCLUSIONS AND RECOMMENDATIONS

#### 5.1 Conclusions

In this study, different synthesis methods in producing modified magnetic biochar were determined for the degradation of organic dyes in wastewater. It was found that there were three commonly used methods, namely, impregnation-pyrolysis, chemical co-precipitation and calcination. Impregnation-pyrolysis was the most commonly used at the present while chemical co-precipitation was found to be the simplest process as it only required mixing and heating processes. Meanwhile, the calcination process was relatively simple to operate and tended to produce materials with controlled size and high magnetism.

On the other hand, the characteristics of the magnetic biochar were investigated. SEM images revealed that the nanoparticles were well distributed on the biochar surface in forming a porous surface. When particles on the biochar surface agglomerated, this led to lower specific surface area and catalytic activity. From the BET surface area results, it was found that the BET surface area decreased in modified biochar compared to pristine biochar. This might be due to the blockages of pore sites or Fe particles filled in some pores thereby decreasing the specific surface area. For FTIR spectra, most of the modified biochar consists of functional groups such as aromatic and heterocyclic carbon compounds. Furthermore, the XRD pattern showed that all of the active components were loaded successfully on the biochar.

Besides, the magnetic biochar catalysts showed good stability and excellent reusability hence had great potential in the degradation of organic dyes. It was found that the degradation efficiency in organic dyes of magnetic biochar catalysts was still high even after reusing multiple cycles whereas the amount of iron leaching for magnetic modified catalyst was less than 2 mg/L, showing its excellent stability.

## 5.2 Recommendations for future work

Although the magnetic biochar catalysts showed promising results in degradation efficiency of organic dyes with AOPs from various journal reviews, there are also many aspects to be enhanced in future research. The comparison of results might not be so accurate as it was affected by different operating conditions due to the research analysis was conducted according to the data obtained from different journal reviews. There were limited published results available to provide sufficient proofs for the effectiveness of modified magnetic biochar catalysts in degrading organic dyes with AOPs. Moreover, improvements can be taken in the future review study to improve the accuracy of the results. Thus, some recommendations for future related review are listed below.

- (i) The catalytic performance of magnetic biochar catalysts decreased after reusing multiple cycles although they possessed good stability. Hence, further research on the magnetic biochar catalysts regeneration methods should be conducted.
- (ii) The characterisation techniques and degradation efficiency of organic dyes should be conducted in the same operating conditions to improve the accuracy in comparing the results.
- (iii) The catalytic mechanism of magnetic biochar catalysts was studied. Nevertheless, the catalytic performance and catalytic effect of biochar and magnetic biochar should be compared to understand more about the difference between using pristine biochar and magnetic biochar.
- (iv) The ratio of metal oxides to biochar should be fixed to improve the accuracy and ease the comparison of the results of the dye degradation efficiency.

## REFERENCES

- Ahmad, A., Khan, N., Giri, B., Chowdhary, P. and Chaturvedi, P., 2020. Removal of methylene blue dye using rice husk, cow dung and sludge biochar: characterization, application, and kinetic studies. *Bioresource Technology*, 306, p.123202.
- Ahmad, A., Mohd-Setapar, S., Chuong, C., Khatoon, A., Wani, W., Kumar, R. and Rafatullah, M., 2015. Recent advances in new generation dye removal technologies: novel search for approaches to reprocess wastewater. *RSC Advances*, 5(39), pp.30801-30818.
- Ahmed, M., Zhou, J., Ngo, H., Guo, W. and Chen, M., 2016. Progress in the preparation and application of modified biochar for improved contaminant removal from water and wastewater. *Bioresource Technology*, 214, pp.836-851.
- Azargohar, R., Nanda, S., Dalai, A. and Kozinski, J., 2019. Physico-chemistry of biochars produced through steam gasification and hydro-thermal gasification of canola hull and canola meal pellets. *Biomass and Bioenergy*, 120, pp.458-470.
- Baban, A., Yediler, A., Avaz, G. and Hostede, S., 2010. Biological and oxidative treatment of cotton textile dye-bath effluents by fixed and fluidized bed reactors. *Bioresource Technology*, 101(4), pp.1147-1152.
- Banik, C., Lawrinenko, M., Bakshi, S. and Laird, D., 2018. Impact of pyrolysis temperature and feedstock on surface charge and functional group chemistry of biochars. *Journal of Environmental Quality*, 47(3), pp.452-461.
- Barakat, M., 2011. New trends in removing heavy metals from industrial wastewater. *Arabian Journal of Chemistry*, 4(4), pp.361-377.
- Butler, E., Hung, Y., Ahmad, M. and Fu, Y., 2016. Treatment and management of industrial dye wastewater for water resources protection. *Natural Resources and Control Processes*, pp.187-232.
- Cárdenas-Aguiar, E., Gascó, G., Paz-Ferreiro, J. and Méndez, A., 2019. Thermogravimetric analysis and carbon stability of chars produced from slow pyrolysis and hydrothermal carbonization of manure waste. *Journal of Analytical and Applied Pyrolysis*, 140, pp.434-443.
- Carrier, M., Hardie, A., Uras, Ü., Görgens, J. and Knoetze, J., 2012. Production of char from vacuum pyrolysis of South-African sugar cane bagasse and its characterization as activated carbon and biochar. *Journal of Analytical and Applied Pyrolysis*, 96, pp.24-32.

Cely, P., Gascó, G., Paz-Ferreiro, J. and Méndez, A., 2015. Agronomic properties of biochars from different manure wastes. *Journal of Analytical and Applied Pyrolysis*, 111, pp.173-182.

Cha, J., Park, S., Jung, S., Ryu, C., Jeon, J., Shin, M. and Park, Y., 2016. Production and utilization of biochar: a review. *Journal of Industrial and Engineering Chemistry*, 40, pp.1-15.

Chan, N., 2012. Managing urban rivers and water quality in Malaysia for sustainable water resources. *International Journal of Water Resources Development*, 28(2), pp.343-354.

Chan, Y., Cheah, K., How, B., Loy, A., Shahbaz, M., Singh, H., Yusuf, N., Shuhaili, A., Yusup, S., Ghani, W., Rambli, J., Kansha, Y., Lam, H., Hong, B. and Ngan, S., 2019. An overview of biomass thermochemical conversion technologies in Malaysia. *Science of The Total Environment*, 680, pp.105-123.

Chen, D., Cheng, Y., Zhou, N., Chen, P., Wang, Y., Li, K., Huo, S., Cheng, P., Peng, P., Zhang, R., Wang, L., Liu, H., Liu, Y. and Ruan, R., 2020a. Photocatalytic degradation of organic pollutants using TiO<sub>2</sub>-based photocatalysts: a review. *Journal of Cleaner Production*, 268, p.121725.

Chen, X., Li, F., Chen, H., Wang, H. and Li, G., 2020b. Fe<sub>2</sub>O<sub>3</sub>/TiO<sub>2</sub> functionalized biochar as a heterogeneous catalyst for dyes degradation in water under Fenton processes. *Journal of Environmental Chemical Engineering*, 8(4), p.103905.

Chia, C., Gong, B., Joseph, S., Marjo, C., Munroe, P. and Rich, A., 2012. Imaging of mineral-enriched biochar by FTIR, Raman and SEM-EDX. *Vibrational Spectroscopy*, 62, pp.248-257.

Claoston, N., Samsuri, A., Ahmad Husni, M. and Mohd Amran, M., 2014. Effects of pyrolysis temperature on the physicochemical properties of empty fruit bunch and rice husk biochars. *Waste Management & Research*, 32(4), pp.331-339.

Cui, J., Zhang, F., Li, H., Cui, J., Ren, Y. and Yu, X., 2020. Recent progress in biochar-based photocatalysts for wastewater treatment: synthesis, mechanisms, and applications. *Applied Sciences*, 10(3), p.1019.

Danish, M., Naqvi, M., Farooq, U. and Naqvi, S., 2015. Characterization of south asian agricultural residues for potential utilization in future 'energy mix'. *Energy Procedia*, 75, pp.2974-2980.

Deng, Y. and Zhao, R., 2015. Advanced oxidation processes (AOPs) in wastewater treatment. *Current Pollution Reports*, 1(3), pp.167-176.

- Ding, W., Dong, X., Ime, I., Gao, B. and Ma, L., 2014. Pyrolytic temperatures impact lead sorption mechanisms by bagasse biochars. *Chemosphere*, 105, pp.68-74.
- Dos Santos, R.F., Ramlow, H., Dolzan, N., Machado, R., de Aguiar, C.R.L. and Marangoni, C., 2018. Influence of different textile fibers on characterization of dyeing wastewater and final effluent. *Environmental Monitoring and Assessment*, 190(11).
- Duan, X., Yang, S., Waclawek, S., Fang, G., Xiao, R. and Dionysiou, D., 2020. Limitations and prospects of sulfate-radical based advanced oxidation processes. *Journal of Environmental Chemical Engineering*, 8(4), p.103849.
- El-gamal, E.H., Saleh, M., Elsokkary, I., Rashad, M. and El-latif, M.M.A., 2017. Comparison between properties of biochar produced by traditional and controlled pyrolysis. *Alexandria Science Exchange Journal: An International Quarterly Journal of Science Agricultural Environments*, 38, pp.412–425.
- Elleuch, A., Boussetta, A., Yu, J., Halouani, K. and Li, Y., 2013. Experimental investigation of direct carbon fuel cell fueled by almond shell biochar: Part I. Physico-chemical characterization of the biochar fuel and cell performance examination. *International Journal of Hydrogen Energy*, 38(36), pp.16590-16604.
- Eltaweil, A., Ali Mohamed, H., Abd El-Monaem, E. and El-Subruti, G., 2020. Mesoporous magnetic biochar composite for enhanced adsorption of malachite green dye: characterization, adsorption kinetics, thermodynamics and isotherms. *Advanced Powder Technology*, 31(3), pp.1253-1263.
- Fang, C., Zhang, T., Li, P., Jiang, R., Wu, S., Nie, H. and Wang, Y., 2015. Phosphorus recovery from biogas fermentation liquid by Ca–Mg loaded biochar. *Journal of Environmental Sciences*, 29, pp.106-114.
- Feng, Z., Yuan, R., Wang, F., Chen, Z., Zhou, B. and Chen, H., 2020. Preparation of magnetic biochar and its application in catalytic degradation of organic pollutants: a review. *Science of The Total Environment*, 765, p.142673.
- Fontecha-Cámara, M., Álvarez-Merino, M., Carrasco-Marín, F., López-Ramón, M. and Moreno-Castilla, C., 2011. Heterogeneous and homogeneous Fenton processes using activated carbon for the removal of the herbicide amitrole from water. *Applied Catalysis B: Environmental*, 101(3-4), pp.425-430.
- Gan, Q., Hou, H., Liang, S., Qiu, J., Tao, S., Yang, L., Yu, W., Xiao, K., Liu, B., Hu, J., Wang, Y. and Yang, J., 2020. Sludge-derived biochar with multivalent iron as an efficient Fenton catalyst for degradation of 4-Chlorophenol. *Science of The Total Environment*, 725, p.138299.

Gao, R., Song, J., Hu, Y., Zhang, X., Gong, S. and Li, W., 2017. Facile synthesis of Ag/Ag<sub>3</sub>PO<sub>4</sub> composites with highly efficient and stable photocatalytic performance under visible light. *Journal of the Chinese Chemical Society*, 64(10), pp.1172-1180.

Gautam, R. and Chattopadhyaya, M., 2016. Advanced oxidation process-based nanomaterials for the remediation of recalcitrant pollutants. *Nanomaterials for Wastewater Remediation*, pp.33-48.

Godwin, P.M., Pan, Y., Xiao, H. and Afzal, M.T., 2019. Progress in preparation and application of modified biochar for improving heavy metal ion removal from wastewater. *Journal of Bioresources and Bioproducts*, 4(1), pp.31-42.

Gong, J., Yao, K., Liu, J., Jiang, Z., Chen, X., Wen, X., Mijowska, E., Tian, N. and Tang, T., 2013. Striking influence of Fe<sub>2</sub>O<sub>3</sub> on the “catalytic carbonization” of chlorinated poly(vinyl chloride) into carbon microspheres with high performance in the photo-degradation of Congo red. *Journal of Materials Chemistry A*, 1(17), p.5247.

Haidich, A.-B., 2014. Meta-analysis in medical research. pp.30-37.

Hameed, B. and El-Khaiary, M., 2008. Kinetics and equilibrium studies of malachite green adsorption on rice straw-derived char. *Journal of Hazardous Materials*, 153(1-2), pp.701-708.

Hansen, V., Müller-Stöver, D., Ahrenfeldt, J., Holm, J., Henriksen, U. and Hauggaard-Nielsen, H., 2015. Gasification biochar as a valuable by-product for carbon sequestration and soil amendment. *Biomass and Bioenergy*, 72, pp.300-308.

Haroun, M. and Idris, A., 2009. Treatment of textile wastewater with an anaerobic fluidized bed reactor. *Desalination*, 237(1-3), pp.357-366.

Hashemian, S., 2013. Fenton-Like oxidation of malachite green solutions: kinetic and thermodynamic Study. *Journal of Chemistry*, 2013, pp.1-7.

He, L., Yang, S., Bai, S., Pang, J., Liu, G., Cao, G., Zhao, L., Feng, X. and Ren, N., 2020. Fabrication and environmental assessment of photo-assisted Fenton-like Fe/FBC catalyst utilizing mealworm frass waste. *Journal of Cleaner Production*, 256, p.120259.

Hox, J. and Boeije, H., 2004. Data collection, primary vs. secondary. *Encyclopedia of Social Measurement*, pp.593-599.

Huang, Y.F., Ang, S.Y., Lee, K.M. and Lee, T.S., 2015. Quality of water resources in Malaysia. In: *Research and Practices in Water Quality*. InTech.

IHS Markit, 2018. *Dyes*. [online] Available at: <<https://ihsmarkit.com/products/dyes-chemical-economics-handbook.html>> [Accessed 18 April 2021].

Islam, T., Peng, C., Ali, I., Li, J., Khan, Z., Sultan, M. and Naz, I., 2020. Synthesis of rice husk-derived magnetic biochar through liquefaction to adsorb anionic and cationic dyes from aqueous solutions. *Arabian Journal for Science and Engineering*, 46(1), pp.233-246.

Jadhav, S., Yedurkar, S., Phugare, S. and Jadhav, J., 2012. Biodegradation studies on Acid Violet 19, a triphenylmethane dye, by *Pseudomonas aeruginosa* BCH. *Clean - Soil, Air, Water*, 40(5), pp.551-558.

Jafri, N., Wong, W., Doshi, V., Yoon, L. and Cheah, K., 2018. A review on production and characterization of biochars for application in direct carbon fuel cells. *Process Safety and Environmental Protection*, 118, pp.152-166.

Jiang, C., Pang, S., Ouyang, F., Ma, J. and Jiang, J., 2010. A new insight into Fenton and Fenton-like processes for water treatment. *Journal of Hazardous Materials*, 174(1-3), pp.813-817.

Jiang, S., Ling, L., Chen, W., Liu, W., Li, D. and Jiang, H., 2019. High efficient removal of bisphenol A in a peroxymonosulfate/iron functionalized biochar system: mechanistic elucidation and quantification of the contributors. *Chemical Engineering Journal*, 359, pp.572-583.

Jilcha Sileyew, K., 2020. Research Design and Methodology. In: *Cyberspace*. IntechOpen. pp.137-144.

Joshi, M., Bhattacharyya, A. and Ali, S.W., 2008. Characterization techniques for nanotechnology applications in textiles. *Indian Journal of Fibre and Textile Research*, 33(3), pp.304-317.

Jun, B., Kim, Y., Yoon, Y., Yea, Y. and Park, C., 2020. Enhanced sonocatalytic degradation of recalcitrant organic contaminants using a magnetically recoverable Ag/Fe-loaded activated biochar composite. *Ceramics International*, 46(14), pp.22521-22531.

Kausar, A., Iqbal, M., Javed, A., Aftab, K., Nazli, Z., Bhatti, H. and Nouren, S., 2018. Dyes adsorption using clay and modified clay: a review. *Journal of Molecular Liquids*, 256, pp.395-407.

Keiluweit, M., Nico, P., Johnson, M. and Kleber, M., 2010. Dynamic molecular structure of plant biomass-derived black carbon (Biochar). *Environmental Science & Technology*, 44(4), pp.1247-1253.

Khataee, A., Kayan, B., Gholami, P., Kalderis, D. and Akay, S., 2017. Sonocatalytic degradation of an anthraquinone dye using TiO<sub>2</sub>-biochar nanocomposite. *Ultrasonics Sonochemistry*, 39, pp.120-128.

Koe, W., Lee, J., Chong, W., Pang, Y. and Sim, L., 2019. An overview of photocatalytic degradation: photocatalysts, mechanisms, and development of photocatalytic membrane. *Environmental Science and Pollution Research*, 27(3), pp.2522-2565.

Lau, W. and Ismail, A., 2009. Polymeric nanofiltration membranes for textile dye wastewater treatment: preparation, performance evaluation, transport modelling, and fouling control: a review. *Desalination*, 245(1-3), pp.321-348.

Lee, Y., Park, J., Ryu, C., Gang, K., Yang, W., Park, Y., Jung, J. and Hyun, S., 2013. Comparison of biochar properties from biomass residues produced by slow pyrolysis at 500°C. *Bioresource Technology*, 148, pp.196-201.

Lei, C., Sun, Y., Tsang, D. and Lin, D., 2018. Environmental transformations and ecological effects of iron-based nanoparticles. *Environmental Pollution*, 232, pp.10-30.

Li, B., Wang, H., Lan, Y., Cui, Y., Zhang, Y., Feng, Y., Pan, J., Meng, M. and Wu, C., 2020a. A controllable floating pDA-PVDF bead for enhanced decomposition of H<sub>2</sub>O<sub>2</sub> and degradation of dyes. *Chemical Engineering Journal*, 385, p.123907.

Li, H., Li, M., Qiu, G., Li, C., Qu, C. and Yang, B., 2015. Synthesis and characterization of MgO nanocrystals for biosensing applications. *Journal of Alloys and Compounds*, 632, pp.639–644.

Li, S., Wang, Z., Zhao, X., Yang, X., Liang, G. and Xie, X., 2019. Insight into enhanced carbamazepine photodegradation over biochar-based magnetic photocatalyst Fe<sub>3</sub>O<sub>4</sub>/BiOBr/BC under visible LED light irradiation. *Chemical Engineering Journal*, 360, pp.600–611.

Li, X., Wang, C., Zhang, J., Liu, J., Liu, B. and Chen, G., 2020b. Preparation and application of magnetic biochar in water treatment: a critical review. *Science of the Total Environment*, 711, p.134847.

Liberati, A., Altman, D.G., Tetzlaff, J., Mulrow, C., Gøtzsche, P.C., Ioannidis, J.P.A., Clarke, M., Devereaux, P.J., Kleijnen, J. and Moher, D., 2009. The Prisma statement for reporting systematic reviews and meta-analyses of studies that evaluate health care interventions: explanation and elaboration. *Journal of clinical epidemiology*, 62(10), pp.e1–e34.

Liu, C., Chen, L., Ding, D. and Cai, T., 2019. From rice straw to magnetically recoverable nitrogen doped biochar: efficient activation of peroxydisulfate for the degradation of metolachlor. *Applied Catalysis B: Environmental*, 254, pp.312–320.

Liu, X., Qiu, M. and Huang, C., 2011. Degradation of the reactive black 5 by Fenton and Fenton-like system. *Procedia Engineering*, 15, pp.4835–4840.

Liu, X., Zhang, Y., Li, Z., Feng, R. and Zhang, Y., 2014. Characterization of corncob-derived biochar and pyrolysis kinetics in comparison with corn stalk and sawdust. *Bioresource Technology*, 170, pp.76–82.

Liu, Z. and Han, G., 2015. Production of solid fuel biochar from waste biomass by low temperature pyrolysis. *Fuel*, 158, pp.159–165.

Lu, A.H., Salabas, E.L. and Schüth, F., 2007. Magnetic nanoparticles: synthesis, protection, functionalization, and application. *Angewandte Chemie - International Edition*, 46(8), pp.1222–1244.

Luo, L., Xu, C., Chen, Z. and Zhang, S., 2015. Properties of biomass-derived biochars: combined effects of operating conditions and biomass types. *Bioresource Technology*, 192, pp.83–89.

Ma, H., Li, J.B., Liu, W.W., Miao, M., Cheng, B.J. and Zhu, S.W., 2015. Novel synthesis of a versatile magnetic adsorbent derived from corncob for dye removal. *Bioresource Technology*, 190, pp.13–20.

Madhav, S., Ahamad, A., Singh, P. and Mishra, P.K., 2018. A review of textile industry: wet processing, environmental impacts, and effluent treatment methods. *Environmental Quality Management*, 27(3), pp.31–41.

Mengist, W., Soromessa, T. and Legese, G., 2020. Method for conducting systematic literature review and meta-analysis for environmental science research. *MethodsX*, 7, p.100777.

Mian, M.M. and Liu, G., 2019. Sewage sludge-derived TiO<sub>2</sub>/Fe/Fe<sub>3</sub>C-biochar composite as an efficient heterogeneous catalyst for degradation of methylene blue. *Chemosphere*, 215, pp.101–114.

- Mian, M., Liu, G., Yousaf, B., Fu, B., Ahmed, R., Abbas, Q., Munir, M. and Ruijia, L., 2019. One-step synthesis of N-doped metal/biochar composite using NH<sub>3</sub>-ambiance pyrolysis for efficient degradation and mineralization of Methylene Blue. *Journal of Environmental Sciences*, 78, pp.29–41.
- Mirzaei, A., Chen, Z., Haghghat, F. and Yerushalmi, L., 2017. Removal of pharmaceuticals from water by homo/heterogonous Fenton-type processes: a review. *Chemosphere*, 174, pp.665–688.
- Nasrollahzadeh, M., Atarod, M., Sajjadi, M., Sajadi, S. and Issaabadi, Z., 2019. Plant-mediated green synthesis of nanostructures: mechanisms, characterization, and applications. *Interface Science and Technology*, pp.199-322.
- Nguyen, V., Van, H., Nguyen, V., Dam, X. Van, Hoang, L. and Ha, L., 2020. Magnetic Fe<sub>3</sub>O<sub>4</sub> nanoparticle biochar derived from pomelo peel for Reactive Red 21 adsorption from aqueous solution. *Journal of Chemistry*, 2020, pp.1-14.
- Nidheesh, P., Gopinath, A., Ranjith, N., Praveen Akre, A., Sreedharan, V. and Suresh Kumar, M., 2020. Potential role of biochar in advanced oxidation processes: A sustainable approach. *Chemical Engineering Journal*, 405, p.126582.
- Oh, S., Seo, Y., Kim, B., Kim, I. and Cha, D., 2016. Microbial reduction of nitrate in the presence of zero-valent iron and biochar. *Bioresource Technology*, 200, pp.891–896.
- Onwuegbuzie, A.J. and Frels, R., 2016. Seven Steps to a comprehensive literature review. *Journal of Educational Social Studies*, 23(2), pp.48–64.
- Pandey, D., Daverey, A. and Arunachalam, K., 2020. Biochar: production, properties and emerging role as a support for enzyme immobilization. *Journal of Cleaner Production*, 255, p.120267.
- Pang, Y.L. and Abdullah, A.Z., 2013. Current status of textile industry wastewater management and research progress in malaysia: a review. *Clean - Soil, Air, Water*, 41(8), pp.751–764.
- Pang, Y.L., Lim, S. and Lee, R.K.L., 2019. Enhancement of sonocatalytic degradation of organic dye by using titanium dioxide (TiO<sub>2</sub>)/ activated carbon (AC) derived from oil palm empty fruit bunch. *Environmental Science and Pollution Research*.
- Pang, Y.L., Lim, S., Ong, H.C. and Chong, W.T., 2016. Research progress on iron oxide-based magnetic materials: synthesis techniques and photocatalytic applications. *Ceramics International*, 42(1), pp.9–34.

Park, J.-H., Wang, J.J., Park, K.H. and Seo, D.-C., 2020. Heterogeneous fenton oxidation of methylene blue with Fe-impregnated biochar catalyst. *Biochar*, 2(2), pp.165–176.

Park, J.H., Wang, J.J., Xiao, R., Tafti, N., DeLaune, R.D. and Seo, D.C., 2018. Degradation of Orange G by Fenton-like reaction with Fe-impregnated biochar catalyst. *Bioresource Technology*, 249, pp.368–376.

Patel, J.P. and Parsania, P.H., 2017. Characterization, testing, and reinforcing materials of biodegradable composites. *Biodegradable and Biocompatible Polymer Composites*, pp.55–79.

Peng, L., Ren, Y., Gu, J., Qin, P., Zeng, Q., Shao, J., Lei, M. and Chai, L., 2014. Iron improving bio-char derived from microalgae on removal of tetracycline from aqueous system. *Environmental Science and Pollution Research*, 21(12), pp.7631–7640.

Pereira Lopes, R. and Astruc, D., 2021. Biochar as a support for nanocatalysts and other reagents: recent advances and applications. *Coordination Chemistry Reviews*, 426, p.213585.

Phan, T., Nikoloski, A., Bahri, P. and Li, D., 2018. Adsorption and photo-Fenton catalytic degradation of organic dyes over crystalline LaFeO<sub>3</sub>-doped porous silica. *RSC Advances*, 8(63), pp.36181-36190.

Prazeres, A.R., Albuquerque, A., Luz, S., Jerónimo, E., Carvalho, F., Centro, C., Agricultura, D., Alimentaria, A., Alentejo, I. and Beja, P. De, 2014. Hydroponic system: a promising biotechnology for food production and wastewater treatment. *Food Biosynthesis*, pp.317-350.

Qian, L., Shang, X., Zhang, B., Zhang, W., Su, A., Chen, Y., Ouyang, D., Han, L., Yan, J. and Chen, M., 2019. Enhanced removal of Cr(VI) by silicon rich biochar-supported nanoscale zero-valent iron. *Chemosphere*, 215, pp.739–745.

Quan, G., Sun, W., Yan, J. and Lan, Y., 2014. Nanoscale zero-valent iron supported on biochar: characterization and reactivity for degradation of Acid Orange 7 from aqueous solution. *Water, Air, and Soil Pollution*, 225(11).

Rajapaksha, A.U., Chen, S.S., Tsang, D.C.W., Zhang, M., Vithanage, M., Mandal, S., Gao, B., Bolan, N.S. and Ok, Y.S., 2016. Engineered/designer biochar for contaminant removal/immobilization from soil and water: potential and implication of biochar modification. *Chemosphere*, 148, pp.276–291.

Rangabhashiyam, S., Anu, N. and Selvaraju, N., 2013. Sequestration of dye from textile industry wastewater using agricultural waste products as adsorbents. *Journal of Environmental Chemical Engineering*, 1(4), pp.629–641.

Reza, M.T., Lynam, J.G., Uddin, M.H. and Coronella, C.J., 2013. Hydrothermal carbonization: fate of inorganics. *Biomass and Bioenergy*, 49, pp.86–94.

Riaz, N., Hassan, M., Siddique, M., Mahmood, Q., Farooq, U., Sarwar, R. and Khan, M.S., 2020. Photocatalytic degradation and kinetic modeling of azo dye using bimetallic photocatalysts: effect of synthesis and operational parameters. *Environmental Science and Pollution Research*, 27(3), pp.2992–3006.

Robinson, T., McMullan, G., Marchant, R. and Nigam, P., 2004. Remediation of dyes in textile effluent: a critical review on current treatment technologies with a proposed alternative. *International Journal of Environment and Pollution*, 21(3), pp.211–222.

Rodriguez Correa, C., Hehr, T., Voglhuber-Slavinsky, A., Rauscher, Y. and Kruse, A., 2019. Pyrolysis vs. hydrothermal carbonization: understanding the effect of biomass structural components and inorganic compounds on the char properties. *Journal of Analytical and Applied Pyrolysis*, 140, pp.137–147.

Rollinson, A.N., 2016. Gasification reactor engineering approach to understanding the formation of biochar properties. *Proceedings of the Royal Society A: Mathematical, Physical and Engineering Sciences*, 472(2192).

Rosal, A.R.R. and Agüera, A., 2008. Ozone-Based Technologies in Water. *Emerging Contaminants from Industrial and Municipal Waste*, pp.127–175.

Rubeena, K.K., Hari Prasad Reddy, P., Laiju, A.R. and Nidheesh, P. V., 2018. Iron impregnated biochars as heterogeneous Fenton catalyst for the degradation of Acid Red 1 dye. *Journal of Environmental Management*, 226, pp.320–328.

Sarkar, B., Mandal, S., Tsang, Y.F., Kumar, P., Kim, K.H. and Ok, Y.S., 2018. Designer carbon nanotubes for contaminant removal in water and wastewater: a critical review. *Science of the Total Environment*, 612, pp.561–581.

Shan, R., Han, J., Gu, J., Yuan, H., Luo, B. and Chen, Y., 2020. A review of recent developments in catalytic applications of biochar-based materials. *Resources, Conservation and Recycling*, 162, p.105036.

Silva, V.A.J., Andrade, P.L., Silva, M.P.C., Bustamante, A.D., De Los Santos Valladares, L. and Albino Aguiar, J., 2013. Synthesis and characterization of Fe<sub>3</sub>O<sub>4</sub> nanoparticles coated with fucan polysaccharides. *Journal of Magnetism and Magnetic Materials*, 343, pp.138–143.

- Sindhu, R., Binod, P. and Pandey, A., 2015. Microbial poly-3-hydroxybutyrate and related copolymers. *Industrial Biorefineries and White Biotechnology*, pp.575-605.
- Singh, J., Sharma, S., Aanchal and Basu, S., 2019. Synthesis of Fe<sub>2</sub>O<sub>3</sub>/TiO<sub>2</sub> monoliths for the enhanced degradation of industrial dye and pesticide via photo-Fenton catalysis. *Journal of Photochemistry and Photobiology A: Chemistry*, 376, pp.32–42.
- Sizmur, T., Fresno, T., Akgül, G., Frost, H. and Moreno-Jiménez, E., 2017. Biochar modification to enhance sorption of inorganics from water. *Bioresource Technology*, 246, pp.34–47.
- Snyder, H., 2019. Literature review as a research methodology: an overview and guidelines. *Journal of Business Research*, 104, pp.333–339.
- Sonawane, G.H., Patil, S.P. and Sonawane, S.H., 2018. Nanocomposites and its applications. *Applications of Nanomaterials*, pp.1-22.
- Sreeja, P.H. and Sosamony, K.J., 2016. A comparative study of homogeneous and heterogeneous photo-Fenton process for textile wastewater treatment. *Procedia Technology*, 24, pp.217–223.
- Subramonian, W., Wu, T.Y. and Chai, S.P., 2017. Photocatalytic degradation of industrial pulp and paper mill effluent using synthesized magnetic Fe<sub>2</sub>O<sub>3</sub>-TiO<sub>2</sub>: treatment efficiency and characterizations of reused photocatalyst. *Journal of Environmental Management*, 187, pp.298–310.
- Tan, X. fei, Liu, Y. guo, Gu, Y. ling, Xu, Y., Zeng, G. ming, Hu, X. jiang, Liu, S. bo, Wang, X., Liu, S. mian and Li, J., 2016. Biochar-based nano-composites for the decontamination of wastewater: a review. *Bioresource Technology*, 212, pp.318–333.
- Thines, K.R., Abdullah, E.C., Mubarak, N.M. and Ruthiraan, M., 2017. Synthesis of magnetic biochar from agricultural waste biomass to enhancing route for waste water and polymer application: a review. *Renewable and Sustainable Energy Reviews*, 67, pp.257–276.
- Tian, Y., Wu, M., Lin, X., Huang, P. and Huang, Y., 2011. Synthesis of magnetic wheat straw for arsenic adsorption. *Journal of Hazardous Materials*, 193, pp.10–16.
- Tomczyk, A., Sokołowska, Z. and Boguta, P., 2020. Biochar physicochemical properties: pyrolysis temperature and feedstock kind effects. *Reviews in Environmental Science and Biotechnology*, 19(1), pp.191–215.

Ubani, C.A. and Ibrahim, M.A., 2019. Complementary processing methods for ZnO nanoparticles. *Materials Today: Proceedings*, 7, pp.646–654.

Uzun, B.B., Apaydin-Varol, E., Ateş, F., Özbay, N. and Pütün, A.E., 2010. Synthetic fuel production from tea waste: characterisation of bio-oil and bio-char. *Fuel*, 89(1), pp.176–184.

Van Zwieten, L., Kimber, S., Morris, S., Chan, K.Y., Downie, A., Rust, J., Joseph, S. and Cowie, A., 2010. Effects of biochar from slow pyrolysis of papermill waste on agronomic performance and soil fertility. *Plant and Soil*, 327(1), pp.235–246.

Verma, Y., 2008. Acute toxicity assessment of textile dyes and textile and dye industrial effluents using *Daphnia magna* bioassay. *Toxicology and Industrial Health*, 24(7), pp.491–500.

Wang, B., Liu, B., Ji, X.X. and Ma, M.G., 2018. Synthesis, characterization, and photocatalytic properties of bamboo charcoal/TiO<sub>2</sub> composites using four sizes powder. *Materials*, 11(5).

Wang, C., Huang, R. and Sun, R., 2020. Green one-spot synthesis of hydrochar supported zero-valent iron for heterogeneous Fenton-like discoloration of dyes at neutral pH. *Journal of Molecular Liquids*, 320.

Wang, H., Yi, H., Zhu, C., Wang, X. and Jin Fan, H., 2015. Functionalized highly porous graphitic carbon fibers for high-rate supercapacitive electrodes. *Nano Energy*, 13, pp.658–669.

Wang, J. and Wang, S., 2019. Preparation, modification and environmental application of biochar: a review. *Journal of Cleaner Production*, 227, pp.1002–1022.

Wang, N., Zheng, T., Zhang, G. and Wang, P., 2016. A review on Fenton-like processes for organic wastewater treatment. *Journal of Environmental Chemical Engineering*, 4(1), pp.762–787.

Wang, S., Zhao, M., Zhou, M., Li, Y.C., Wang, J., Gao, B., Sato, S., Feng, K., Yin, W., Igalavithana, A.D., Oleszczuk, P., Wang, X. and Ok, Y.S., 2019a. Biochar-supported nZVI (nZVI/BC) for contaminant removal from soil and water: a critical review. *Journal of Hazardous Materials*, 373, pp.820–834.

Wang, S., Zhao, M., Zhou, M., Zhao, Y., Li, Y.C., Gao, B., Feng, K., Yin, W., Ok, Y.S. and Wang, X., 2019b. Biomass facilitated phase transformation of natural hematite at high temperatures and sorption of Cd<sup>2+</sup> and Cu<sup>2+</sup>. *Environment International*, 124, pp.473–481.

- Weber, K. and Quicker, P., 2018. Properties of biochar. *Fuel*, 217, pp.240–261.
- Weng, X., Lin, S., Zhong, Y. and Chen, Z., 2013. Chitosan stabilized bimetallic Fe/Ni nanoparticles used to remove mixed contaminants-amoxicillin and Cd (II) from aqueous solutions. *Chemical Engineering Journal*, 229, pp.27–34.
- Wu, W., Wu, Z., Yu, T., Jiang, C. and Kim, W.S., 2015. Recent progress on magnetic iron oxide nanoparticles: synthesis, surface functional strategies and biomedical applications. *Science and Technology of Advanced Materials*, 16(2), p.23501.
- Xiang, W., Zhang, X., Chen, J., Zou, W., He, F., Hu, X., Tsang, D.C.W., Ok, Y.S. and Gao, B., 2020. Biochar technology in wastewater treatment: a critical review. *Chemosphere*, 252, p.126539.
- Xiao, R., Wang, J.J., Li, R., Park, J., Meng, Y., Zhou, B., Pensky, S. and Zhang, Z., 2018. Enhanced sorption of hexavalent chromium [Cr(VI)] from aqueous solutions by diluted sulfuric acid-assisted MgO-coated biochar composite. *Chemosphere*, 208, pp.408–416.
- Xu, S., Li, J., Yin, Z., Liu, S., Bian, S. and Zhang, Y., 2020. A highly efficient strategy for enhancing the adsorptive and magnetic capabilities of biochar using Fenton oxidation. *Bioresource Technology*, 315, p.123797.
- Yaashikaa, P.R., Kumar, P.S., Varjani, S. and Saravanan, A., 2020. A critical review on the biochar production techniques, characterization, stability and applications for circular bioeconomy. *Biotechnology Reports*, 28.
- Yan, L., Kong, L., Qu, Z., Li, L. and Shen, G., 2015. Magnetic biochar decorated with ZnS nanocrystals for Pb (II) removal. *ACS Sustainable Chemistry and Engineering*, 3(1), pp.125–132.
- You, S., Ok, Y.S., Chen, S.S., Tsang, D.C.W., Kwon, E.E., Lee, J. and Wang, C.H., 2017. A critical review on sustainable biochar system through gasification: energy and environmental applications. *Bioresource Technology*, 246, pp.242–253.
- Yu, J.X., Wang, L.Y., Chi, R.A., Zhang, Y.F., Xu, Z.G. and Guo, J., 2013. Competitive adsorption of Pb<sup>2+</sup> and Cd<sup>2+</sup> on magnetic modified sugarcane bagasse prepared by two simple steps. *Applied Surface Science*, 268, pp.163–170.
- Yuan, J.H., Xu, R.K. and Zhang, H., 2011. The forms of alkalis in the biochar produced from crop residues at different temperatures. *Bioresource Technology*, 102(3), pp.3488–3497.

Zama, E.F., Zhu, Y.G., Reid, B.J. and Sun, G.X., 2017. The role of biochar properties in influencing the sorption and desorption of Pb(II), Cd(II) and As(III) in aqueous solution. *Journal of Cleaner Production*, 148, pp.127–136.

Zang, T., Wang, H., Liu, Y., Dai, L., Zhou, S. and Ai, S., 2020. Fe-doped biochar derived from waste sludge for degradation of Rhodamine B via enhancing activation of peroxymonosulfate. *Chemosphere*, 261, p.127616.

Zhang, C., Liu, L., Zhao, M., Rong, H. and Xu, Y., 2018a. The environmental characteristics and applications of biochar. *Environmental Science and Pollution Research*, 25(22), pp.21525–21534.

Zhang, G., Qu, J., Liu, H., Cooper, A.T. and Wu, R., 2007. CuFe<sub>2</sub>O<sub>4</sub>/activated carbon composite: a novel magnetic adsorbent for the removal of acid orange II and catalytic regeneration. *Chemosphere*, 68(6), pp.1058–1066.

Zhang, H., Xue, G., Chen, H. and Li, X., 2018b. Magnetic biochar catalyst derived from biological sludge and ferric sludge using hydrothermal carbonization: preparation, characterization and its circulation in Fenton process for dyeing wastewater treatment. *Chemosphere*, 191, pp.64–71.

Zhang, J., Tian, B., Wang, L., Xing, M. and Lei, J., 2018c. Mechanism of photocatalysis. *Lecture Notes in Chemistry*, pp.1–15.

Zhang, J., Zhong, Z., Zhao, J., Yang, M., Li, W. and Zhang, H., 2012. Study on the preparation of activated carbon for direct carbon fuel cell with oak sawdust. *Canadian Journal of Chemical Engineering*, 90(3), pp.762–768.

Zhao, S.X., Ta, N. and Wang, X.D., 2017. Effect of temperature on the structural and physicochemical properties of biochar with apple tree branches as feedstock material. *Energies*, 10(9).

Zheng, Q., Yang, L., Song, D., Zhang, S., Wu, H., Li, S. and Wang, X., 2020. High adsorption capacity of Mg–Al-modified biochar for phosphate and its potential for phosphate interception in soil. *Chemosphere*, p.127469.

Zhu, D., Chen, Y., Yang, H., Wang, S., Wang, X., Zhang, S. and Chen, H., 2020. Synthesis and characterization of magnesium oxide nanoparticle-containing biochar composites for efficient phosphorus removal from aqueous solution. *Chemosphere*, 247, p.125847.

Zhu, D. and Zhou, Q., 2019. Action and mechanism of semiconductor photocatalysis on degradation of organic pollutants in water treatment: a review. *Environmental Nanotechnology, Monitoring and Management*, 12, p.100255.

Zhu, S., Ho, S.H., Huang, X., Wang, D., Yang, F., Wang, L., Wang, C., Cao, X. and Ma, F., 2017. Magnetic nanoscale zerovalent iron assisted biochar: interfacial chemical behaviors and heavy metals remediation performance. *ACS Sustainable Chemistry and Engineering*, 5(11), pp.9673–9682.